# Contents

# 1 Introduction

When modelling prices of financial assets, modelling the volatility process itself plays a crucial role. For the price of an asset $S_t$ price dynamics are often given by a stochastic volatility model driven by a Brownian motion on the form

$$dS_t = \mu_t S_t dt + \sigma_t S_t dB_t \tag{1}$$

where $\mu_t$ is a drift term and $B_t$ is a one-dimensional Brownian motion. The term $\sigma_t$ represents the volatility process, and it is a very important ingredient in the model . However, modelling the volatility process itself is also a complex task. Different approaches to estimate $\sigma_t$ is used throughout the literature. In the simplest models, the volatility is either constant or a deterministic function of time but in most models the volatility process is modelled as a stochastic process itself Gatheral et al. [2018].

Various authors have proposed various approaches to modelling volatility. The use of fractional Brownian motions and fractional Gaussian noise in volatility modelling was in early applications such as Bollerslev and Mikkelsen [1996] and Comte and Renault [1998] introduced to model long-range dependence in financial time series. A well-known example of such a fractional stochastic volatility model is the one proposed by Comte and Renault [1998] who models the dynamics of the volatility $\sigma_t$ of an asset as:

$$Z_t = \ln \sigma_t, \quad dZ_t = -\gamma Z_t dt + \theta dB_t^H$$

where $B^H$ is a fractional Brownian motion with Hurst exponent $H$. The long range dependence is modelled by choosing $1 > H > \frac{1}{2}$ Comte and Renault [1998]. Fractional Brownian motions can be useful building blocks in stochastic volatility models for several reasons. Firstly, a fractional Brownian motion has the ability to model long range dependence which is measured by the slow decay $T^{2H-2}$ of auto-correlation of functions. Secondly, it can generate trajectories of varying level of roughness (Hölder regularity) which is also governed by the Hurst exponent $H$. The long-range dependence is manifested over long time scales while roughness is manifested over short time scales. These two properties are therefore very different, and are not necessarily related. However, for a fractional Brownian motion they are linked through self-similarity and are both governed by the Hurst exponent $H$.

In more recent literature starting with Gatheral et al. [2018], it has been suggested to use fractional stochastic volatility models with $H < \frac{1}{2}$ for modelling volatility. Processes driven by a fractional Brownian motion with $H < \frac{1}{2}$ are referred to as 'rough processes' since these fractional Brownian motion have trajectories rougher than a standard Brownian motion. The reasoning for the choice of $H < \frac{1}{2}$ rely on empirical estimates of the roughness of realized volatility over short intraday time scales. Gatheral et al. [2018] asses the roughness of realized volatility and find that realized volatility exhibit rough behaviour and concludes that 'volatility is rough'. Since then several rough fractional stochastic volatility models have been suggested such as the rough Heston model El Euch et al. [2019] and the rough Bergomi model Bayer et al. [2016] using a Hurst exponent $H$ near 0.1.

In practice, true spot volatility of the underlying model cannot be observed. Only realized volatility can be observed. Therefore, one cannot necessarily conclude that true spot volatility is rough just because realized volatility exhibit rough behaviour. Fukasawa et al. [2022] and Cont and Das [2024] show that estimation errors when estimating volatility can substantially distort the outcome of roughness estimation and lead to a downward bias in the measurement of roughness such that realized volatility appears to be rough even when instantaneous volatility is not.

To overcome this problem of "illusive roughness" caused by volatility discretization error, roughness estimators taking into account and controlling the measurement error have been introduced by Han and Schied [2023] and Bolko et al. [2023]. Both of these estimators take cumulative integrated variance as input.

In this thesis, we extend the analysis from Cont and Das [2024] and investigate further if there is statistical evidence to conclude that 'volatility is rough'. We use the roughness estimators described in both Cont and Das [2024] and Gatheral et al. [2018] to asses the validity of roughness estimates based on realized volatility through detailed simulation studies. Furthermore, we introduce the sequential scale roughness estimator from Han and Schied [2023] to our numerical examples which take cumulative integrated variance as input. We investigate the performance of all three estimators for measuring the roughness of sample paths of stochastic processes based on fractional Brownian motions and other stochastic processes. We then estimate the roughness from realized volatility signals and cumulative realized variance based on high-frequency observations.

Our results are broadly consistent with the findings of Cont and Das [2024]. When using our two roughness estimators that take instantaneous or realized volatility as input, we find that even when instantaneous volatility has diffusive dynamics or is smooth (i.e. $H \geq \frac{1}{2}$) realized volatility exhibits rough behaviour corresponding to a Hurst exponent much smaller than 0.5. In all our numerical examples realized volatility is estimated to be rough no matter what the true roughness of the underlying model is. Especially, we show that in some cases diffusive models or even smooth processes are consistent with an apparent Hurst exponent $H \simeq 0.1$ for realized volatility, similar to the values reported in empirical studies in 'rough volatility' literature. This indicates that the claim 'volatility is rough' is far from an established fact.

For the sequential scale estimator, we find that it performs well when integrated variance approximated directly from instantaneous volatility is used as

input. With minor modifications, the estimator also performs reasonably well when using realized variance as input. In particular, for diffusive models, it estimates the true roughness with high accuracy.
However, the sequential scale estimator remains somewhat susceptible to estimation errors in the cumulative integrated variance. Although this estimation error is small, it is sufficient to distort the outcome of the roughness estimation. Specifically, for smooth processes (i.e., $H > \frac{1}{2}$), the roughness estimates derived from realized variance are often near 0.5, suggesting diffusive behaviour. Similarly, rough processes are estimated to be closer to diffusive behaviour (i.e., $H = \frac{1}{2}$) than they actually are.
Thus, while we do not observe 'illusory roughness' in realized data when using the sequential scale estimator, it does not fully mitigate the distortion caused by estimation errors.

# 2 Fractional Brownian motion

Fractional Brownian motions work well as building blocks for stochastic volatility models. In this section, we will define the fractional Brownian motion, and briefly discuss some of fBm's most important properties. The definitions and properties will mainly follow the theory in Biagini [2008].

A fractional Brownian motion (fBm for short) $(B_t^H)_{t\in\mathbb{R}}$ with Hurst parameter $H \in (0, 1)$ is a centered continuous Gaussian process with covariance function

$$\mathbb{E}\left[B_t^H B_s^H\right] = \frac{1}{2}\left(t^{2H} + S^{2H} - |t-s|^{2H}\right) \tag{2}$$

for $s, t \geq 0$. For $H = \frac{1}{2}$ the fractional Brownian motion reduces to an ordinary Brownian motion. The incremental process of a fractional Brownian motion is called fractional Gaussian noise.
From (2) it can be seen that a fractional Brownian motion has the following properties:

1. $B_0^H = 0$ and $\mathbb{E}[B_t^H] = 0$ for all $t \geq 0$.
2. $B^H$ has homogeneous increments i.e. $B_{t+s}^H - B_s^H$ has the same law of $B_t^H$ for $s, t \geq 0$.
3. $B^H$ is a Gaussian process and $\mathbb{E}[(B_t^H)^2] = t^{2H}$, $t \geq 0$ for all $H \in (0, 1)$.
4. $B^H$ has continuous trajectories.

The fractional Brownian motion can be divided into three very different families corresponding to $0 < H < \frac{1}{2}$, $H = \frac{1}{2}$ and $\frac{1}{2} < H < 1$. Looking at the correlation between two increments, we have that for $H = \frac{1}{2}$ the increments are independent since it is a Brownian motion. For $H \neq \frac{1}{2}$ the increments are not independent.

From (2) it can be seen that the covariance between the increments $B^H_{t+h} - B^H_t$ and $B^H_{s+h} - B^H_s$ with $s + h \leq t$ and $t - s = nh$ is

$$\rho_H(n) = \frac{1}{2} h^{2H} \left( (n+1)^{2H} + (n-1)^{2H} - 2n^{2H} \right).$$

In particular, we have for $n = 1$ meaning two increments of the form $B^H_{t+h} - B^H_t$ and $B^H_{t+2h} - B^H_{t+h}$ that the increments are positively correlated for $H > \frac{1}{2}$ and negatively correlated for $H < \frac{1}{2}$.
When $h = 1$ meaning that the incremental process has time step 1 we have that

$$\rho_H(n) = \frac{1}{2} \left( (n+1)^{2H} + (n-1)^{2H} - 2n^{2H} \right) \sim H(2H-1)n^{2H-2}$$

as $n \to \infty$. Thus, we see that $\sum_{n=1}^{\infty} \rho_H(n) = \infty$ for $H > \frac{1}{2}$ and $\sum_{n=1}^{\infty} |\rho_H(n)| < \infty$ for $H < \frac{1}{2}$. The non-summable autocovariance function in the case $H > \frac{1}{2}$ is equivalent to long-range dependence and it indicates slow decay of the covariance function. That is, for $H > \frac{1}{2}$ the fBm has long-range dependence but for $H < \frac{1}{2}$ it does not.

Furthermore, we have that the covariance function of the fBm is homogeneous of order $2H$. That is,

$$\mathbb{E}\left[ B^H_{at} B^H_{as} \right] = a^{2H} \mathbb{E}\left[ B^H_t B^H_s \right].$$

That implies that $B^H_{at}$ has the same distribution law as $a^{-H} B^H_t$ for all $H \in (0, 1)$. This is known as statistical self-similarity with Hurst index $H$.

Furthermore, it can be shown that $B^H_t$ is almost surely Hölder continuous of order $\alpha$ for any $\alpha < H$. Hölder continuity is also known as Hölder regularity or simply as the roughness or smoothness of a sample path. Therefore, the roughness of $B^H_t$ completely follows the Hurst exponent $H$. Thus, we have that a fractional Brownian motion with Hurst exponent $\frac{1}{2} < H < 1$ has long range dependence in increments and trajectories smoother than a Brownian motion while for $0 < H < \frac{1}{2}$ the fBm has negatively correlated increments (without long range dependence) and trajectories rougher than a Brownian motion Biagini [2008].

In this thesis, we will be simulating high-frequency data based on fractional Brownian motions when performing numerical experiments. Exact simulation of a fractional Brownian motion is computationally challenging, and we will in this thesis simulate paths from the fBm by using a spectral method. More details on this method is described in Appendix 6.1.

# 3 Estimating the roughness of volatility

Measuring the roughness of volatility is in practice not an easy task. In practice, we observe only a singe price path with discrete observation times, and we need to determine the roughness of this path sampled at high frequency. In order to design proper estimators it is crucial to be able to determine the roughness of realized volatility, and multiple ways of measuring the roughness exist in literature. In this section we will introduce three different roughness estimators and the theory behind them. Firstly, we will be using the roughness index estimator via $p$-th variation $\widehat{H}_{L,K}$ which was first introduced by Cont and Das [2024]. Secondly, we will describe the roughness estimator via log regression $\widehat{H}_R$ introduced by Gatheral et al. [2018]. Thirdly, we will be using the sequential scale estimator $\widehat{\mathscr{R}}_n^s$ originally developed by Han and Schied [2023]. The explained theory and rationale behind the estimators will closely follow the theory from the original articles. In Section 4 we will conduct numerical experiments, and we will compare the performance of the three roughness estimators.

### 3.1 Instantaneous volatility and realized volatility

Before we introduce the details of our roughness estimators we will start by explaining the concepts of instantaneous volatility and realized volatility. As mentioned in (1) price dynamics are often modelled on the form

$$dS_t = \mu_t S_t dt + \sigma_t S_t dB_t.$$

The term $\sigma_t$ represents the volatility process, and $\sigma_t$ is also called instantaneous volatility or spot volatility. Thus, instantaneous volatility $\sigma_t$ is the true volatility of the underlying model. In stochastic volatility models, $\sigma_t$ is represented as a stochastic process itself often driven by a Brownian motion or a fractional process. Contrary to prices of an asset, instantaneous volatility cannot be directly observed and needs to be estimated from prices.

In a practical situation, the price of the asset $S_t$ at time $t$ is usually observed over a non-uniform time grid of $[0, T]$:

$$\pi^n = \left(0 = t_0^n < t_1^n < ... < t_{N(\pi^n)}^n = T\right)$$

where $n$ is the sample frequency and $N(\pi^n)$ denotes the number of intervals in the partition $\pi^n$. In order to study high-frequency asymptotics of roughness estimators, it is often assumed that

$$|\pi^n| := \sup_{i=1,\ldots,N(\pi^n)} |t_i^n - t_{i-1}^n| \overset{n\to\infty}{\longrightarrow} 0. \tag{3}$$

That is, the size of the largest interval of $\pi^n$ will converge to 0 as $n \to \infty$ where $n$ can be thought of as a sampling frequency i.e. the number of samples per second (or per other unit).

Instantaneous volatility $\sigma_t$ can then be recovered from integrated variance or quadratic variation of log-prices $\log S$ along this time grid by

$$\sigma_t^2 = \frac{d}{dt}[\log S]_\pi(t)$$

where the quadratic variation of the log-price $[\log S]_\pi(t)$ is defined as

$$[\log S]_\pi(t) = \lim_{n\to\infty} \sum_{\pi^n\cap[0,t]} \left(\log \frac{S(t_{i+1}^n)}{S(t_i^n)}\right)^2 = \lim_{n\to\infty} RV_t^2(\pi^n)^2$$

where $RV_t^2(\pi^n)^2$ is realized variance along the sampling grid $\pi^n$. Hence, $\sigma_t$ can be recovered from a high-frequency limit of realized variance where the realized variance along the sampling grid $\pi_n$, $RV_t^2(\pi^n)^2$, is defined as

$$RV_t(\pi^n)^2 = \sum_{\pi^n\cap[0,t]} \left(\log \frac{S(t_{i+1}^n)}{S(t_i^n)}\right)^2. \tag{4}$$

We then simply define realized volatility as the square root of realized variance. This leads to the following formal definition:

**Definition 1.** *Realized volatility of a price process $S$ over the time interval $[t, t+\Delta]$ along the sampling grid $\pi^n$ is defined as*

$$RV_{t,t+\Delta}(\pi^n) = \sqrt{\sum_{\pi^n\cap[t,t+\Delta]} \left(\log \frac{S(t_{i+1}^n)}{S(t_i^n)}\right)^2}.$$

If the price $S_t$ is a continuous semimartingale then the quadratic variation equals the integrated variance of $\log S$ which is given by

$$\langle logS \rangle_t = \int_0^t \sigma_s^2 ds. \tag{5}$$

Furthermore, if $S_t$ follows a stochastic volatility model given by price dynamics as in (1), it is known that the realized variance converges in probability to the integrated variance of $\log S$ as sampling frequency increases Jacod [2012]. That is,

$$RV_t^2(\pi^n)^2(\pi^n) \xrightarrow[n\to\infty]{\mathbb{P}} \int_0^t \sigma_s^2 ds.$$

From that we immediately obtain that realized volatility converges to

$$RV_{t,t+\Delta}(\pi^n) \xrightarrow[n\to\infty]{\mathbb{P}} \sqrt{\int_t^{t+\Delta} \sigma_s^2 ds}.$$

Hence, along a single price path observed at high-frequency, we can compute the realized volatility as in Definition 1 and use this as an indicator of volatility

$$RV_{t,t+\Delta}(\pi^n) \simeq \sqrt{\Delta}\sigma_t.$$

More precisely, rescaled realized volatility $\frac{1}{\sqrt{\Delta}} RV_{t,t+\Delta}$ can be used as proxy values $\hat{\sigma}_t$ of instantaneous volatility $\sigma_t$. As $n$ increases the estimation becomes more accurate Cont and Das [2024].

Several empirical studies including Gatheral et al. [2018] have attempted to estimate roughness of volatility by estimating the roughness of realized volatility signals (i.e. proxy values $\hat{\sigma}_t$) using high-frequency data. Since carried out on high-frequency data, it is then assumed that the difference between $\hat{\sigma}_t$ and $\sigma_t$ is relatively small, and that the estimated roughness of realized volatility signals also works as a good estimation of the roughness of the instantaneous volatility process $\sigma_t$. However, there is no guarantee that $\hat{\sigma}_t$ and $\sigma_t$ exhibits same kind of roughness behaviour, and as we will illustrate later on estimation error in proxy values $\hat{\sigma}_t$ can substantially distort the roughness estimation.

## 3.2 Roughness index estimator via $p$-th variation

In this section, we will describe the roughness index estimator via normalized $p$-th variation which was introduced in Cont and Das [2024]. We will closely follow the theory and methodology behind the estimator described in Cont and Das [2024].

We are working with partitions of our time interval. Consider a sequence of partitions $\pi = (\pi^n)_{n \geq 1}$ of $[0, T]$ where

$$\pi^n = \left(0 = t_0^n < t_1^n < \ldots < t_{N(\pi^n)}^n = T\right)$$

represents observation times at frequency $n$. We again let $N(\pi^n)$ denotes the number of intervals in the partition $\pi^n$. We assume that assumption (3) is fulfilled for all time partitions considered. That is, the size of the largest interval of $\pi^n$ will converge to 0 as the sampling frequency increases $n \to \infty$.

We will now define the concept of $p$-th variation along a sequence of partitions $(\pi^n)_{n \geq 1}$:

**Definition 2.** (p-th variation along a sequence of partitions)
*$x \in C^0([0,T], \mathbb{R})$ has finite p-th variation along the sequence of partitions $\pi = (\pi^n, n \geq 1)$ if there exists a continuous increasing function $[x]_\pi^{(p)} : [0,T] \to \mathbb{R}_+$ such that*

$$\forall t \in [0, T], \qquad \sum_{\{t_j^n, t_{j+1}^n\} \in \pi^n : t_j^n \leq t} |x(t_{j+1}^n) - x(t_j^n)|^p \overset{n \to \infty}{\longrightarrow} [x]_\pi^{(p)}(t). \tag{6}$$

*If this property holds, then the convergence in (6) is uniform. We call $[x]_\pi^{(p)}$ the p-th variation of $x$ along the sequence of partitions $\pi$. We denote $V_\pi^p([0,T], \mathbb{R})$ the set of all continuous paths with finite p-th variation along $\pi$.*

The concept of roughness will then be formalized using the notion of variation index and roughness index.

**Definition 3.** (Variation index)
*The variation index of a path $x$ along a partition sequence $\pi$ is defined as the smallest $p \geq 1$ for which $x$ has finite $p$-th variation along $\pi$:*

$$p^{\pi}(x) = \inf\left\{p \geq 1 : x \in V_{\pi}^{p}([0,T], \mathbb{R})\right\}.$$

**Definition 4.** (Roughness index)
*The roughness index of a path $x$ (along $\pi$) is defined as*

$$H^{\pi}(x) = \frac{1}{p^{\pi}(x)}.$$

When the underlying sequence of partitions is clear, we will simply denote these indexes as $p(x)$ and $H(x)$.

For a real-valued stochastic process $X : [0,T] \times \Omega \to \mathbb{R}$ the variation index $p^{\pi}(X(., \omega))$ of each sample path $X(., \omega)$ may in principle be different. However, there are many important classes of stochastic processes which have an almost-sure roughness index. For example we have that along the dyadic partition sequence

$$\pi^n = \left(t_i^n = \frac{iT}{2^n}, i = 0, 1, ..., 2^n\right), \tag{7}$$

the fractional Brownian motion $B_t^H$ has roughness index $H^{\pi}(x) = H$ matching the Hurst exponent $H$ and the Hölder regularity Cont and Das [2024].
However, existence of variation index is in general not obvious. Further details can be seen in Han and Schied [2022a].

When estimating roughness from empirical data based on discrete observations, using the $p$-th variation directly is difficult since it involves checking convergence to an unknown limit. To this end, Cont and Das [2024] introduce the concept of normalized $p$-th variation which has better asymptotics:

**Definition 5.** (Normalized p-th variation along a sequence of partitions)
*Let $\pi$ be a sequence of partitions of $[0,T]$ with mesh $|\pi^n| \to 0$ and $\pi^n = \{0 = t_1^n < t_2^n < \cdots < t_{N(\pi^n)}^n = T\}$. $x \in V_{\pi}^{p}([0,T], \mathbb{R})$ is said to have normalized $p$-th variation along $\pi$ if there exists a continuous function $w(x,p,\pi) : [0,T] \to \mathbb{R}$ such that:*

$$\forall t \in [0,T], \qquad \sum_{\pi^n \cap [0,t]} |x(t_{j+1}^n) - x(t_j^n)|^p \to w(x,p,\pi)(t).$$

Cont and Das [2024] justify the terminology by a result that shows that for a large class of functions with $p$-th variation, the normalized $p$-th variation exists and is linear. Furthermore, it can be shown that the normalized $p$-th variation is a 'sharp' statistic meaning that if a function has finite $p$-th variation then for all $q \neq p$ the normalized $p$-th variation is either zero or infinite. Additionally, it is shown that a fractional Brownian motion has normalized $p$-th variation along the dyadic partition $\pi^n$ as in (7) almost-surely.

#### 3.2.1 Estimating the roughness from discrete observations

With these concepts defined we now proceed to explaining how roughness can be estimated from discrete observations. Given discrete observations on a refining partition $\pi^L$ we define the 'normalized $p$-th variation statistic' which is the discrete counterpart of the normalized $p$-th variation as

$$W(L,K,\pi,p,t,X) := \sum_{\pi^K \cap [0,t]} \frac{|X(t_{i+1}^K) - X(t_i^K)|^p}{\sum_{\pi^L \cap [t_i^K, t_{i+1}^K]} |X(t_{j+1}^L) - X(t_j^L)|^p} \times (t_{i+1}^K - t_i^K). \tag{8}$$

This definition involves two frequencies $K$ and $L >> K$. We can consider $L$ as the sample frequency while $K$ is a block frequency such that $\pi^K$ is a subpartition of $\pi^L$. Thus, we are grouping the sample size $L$ into $K$ many groups where each group contains exactly $\frac{L}{K}$ consecutive points. It can be seen that the normalized $p$-th variation statistic converges to the normalized $p$-th variation as $L$ and $K$ increase. That is,

$$\lim_{K\to\infty} \lim_{L\to\infty} W(L,K,\pi,p,t,X) = w(x,p,\pi)(t).$$

The variation index estimator $\hat{p}_{L,K}^{\pi}(X)$ associated with data sampled on $\pi^L$ can then be obtained by computing $W(L,K,\pi,p,t,X)$ for different values of $p$ such that the following equation can be solved for $p_{L,K}^{\pi}(X)$

$$W(L,K,\pi,\hat{p}_{L,K}^{\pi}(X),t,X) = T. \tag{9}$$

The corresponding roughness index estimator is then defined as

$$\hat{H}_{L,K}^{\pi}(X) = \frac{1}{\hat{p}_{L,K}^{\pi}(X)}.$$

If the underlying dataset and partition is clear we will also denote this estimator simply as $\widehat{H}_{L,K}$. We will refer to $\widehat{H}_{L,K}$ as the roughness index estimator via $p$-th variation.

#### 3.2.2 Sample behaviour of $\widehat{H}_{L,K}$

We will now study the behaviour of the roughness estimator based on high-frequency simulated data. We will be simulating from a fractional Brownian motion $B_t^H$ where the true roughness is known to be $H$. For the simulated paths we then compute the roughness index estimator via $p$-th variation $\widehat{H}_{L,K}$ and investigate its performance. We will in these examples be using a uniform partition of the time interval $[0, 1]$ with

$$\pi^n = \left(0 < \frac{1}{n} < \frac{2}{n} < ... < 1\right).$$

We generate data from four fractional Brownian motions with different Hurst exponents $H = \{0.1, 0.3, 0.5, 0.8\}$. For every simulated path we compute the statistic $W(L = 300 \times 300, K = 300, \pi, p, t = 1, X = B^H)$ for different values of $p$. Thus, we use $\pi^L$ as our partition of time and generate $L = 300 \times 300$ points uniformly on the interval $[0, 1]$.
The roughness estimator $\widehat{H}_{L,K}$ solves equation (9) with $T = 1$. To visualize this we plot $\log(W(L = 300 \times 300, K = 300, \pi, p, t = 1, X = B^H))$ against $H = 1/p$. The results are presented in Figure 1. The solid black line is the value of $\log(W(L = 300 \times 300, K = 300, \pi, p, t = 1, X = B^H))$ for different values of $1/p$. The blue vertical line represents the estimated roughness index whereas the black dotted vertical line represent the true Hurst parameter of the underlying model. The blue horizontal line represents $W(L, K, \pi, p, t, X) = 1$ which is the equation $\widehat{H}_{L,K}$ solves. Thus, the estimated roughness index $\widehat{H}_{L,K}$ is found in the crossing between $\log(W(L = 300 \times 300, K = 300, \pi, p, t = 1, X = B^H))$ (solid black line) and $W(L, K, \pi, p, t, X) = 1$ (blue horizontal line).

We now repeat the estimation procedure for 150 independent sample paths using again $W(L = 300 \times 300, K = 300, \pi, p, t = 1, X = B^H)$. In Figure 2 we have generated histograms of the final estimates $\widehat{H}_{L,K}$ for these 150 independent paths. In addition to this, we provide the corresponding summary statistics of the estimated roughness index $\widehat{H}_{L,K}$ for the 150 paths in Table 1.

Figure 1, 2 and Table 1 all indicate that the estimated roughness index via $p$-th variation $\widehat{H}_{L,K}$ seems to be a fairly accurate roughness estimator when used on a data set with of $L = 300 \times 300$ generated from the fractional Brownian motion. All the roughness estimates $\widehat{H}_{L,K}$ are within a distance 0.05 from the true Hurst parameter as seen in Figure 2. The mean and median of the estimated roughness provided in Table 1 are in all four cases very close to the true Hurst parameter. However, for the fBm with Hurst parameter $H = 0.8$ even the upper quartile of $\widehat{H}_{L,K}$ is smaller than the true Hurst parameter. This suggest that the estimated roughness index might be slightly biased downwards in the case of $H = 0.8$. The estimate is, however, still quite accurate also for $H = 0.8$, and we conclude that the roughness estimator $\widehat{H}_{L,K}$ performs very well in these simulation examples.

We now set $L = 2000 \times 2000$ and $K = 2000$, and simulate data from a fBm with Hurst parameter $H = 0.1$. We compute $\hat{H}_{L,K}$ and as before we generate a histogram of the roughness estimates based on 150 independent paths. The

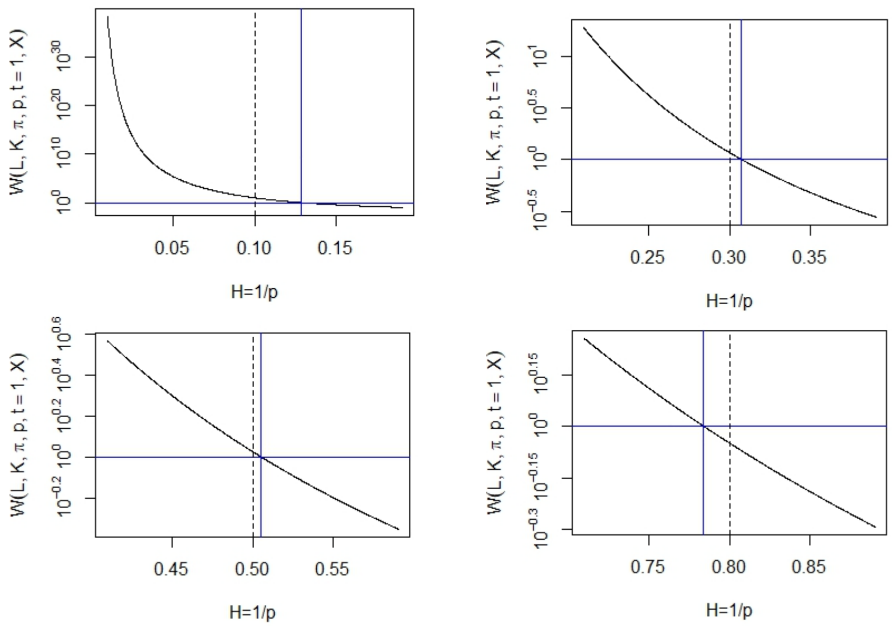


Figure 1: Log-scale plot of the normalized $p$-th variation statistic for fBm with Hurst parameter $H = \{0.1, 0.3, 0.5, 0.8\}$. The black solid line represents the value of $\log(W(L = 300 \times 300, K = 300, \pi, p, t = 1, X = B^H))$ plotted against $H = 1/p$. The blue vertical line represents $\widehat{H}_{L,K}$ using the normalized $p$-th variation statistic with $L = 300 \times 300$ and $K = 300$. The vertical black dotted line represents the true Hurst parameter.

| H | Min. | Lower quartile | Median | Mean | Upper quartile | Max. |
|---|---|---|---|---|---|---|
| 0.1 | 0.0622 | 0.0944 | 0.1021 | 0.1031 | 0.1149 | 0.1402 |
| 0.3 | 0.2746 | 0.2954 | 0.3012 | 0.3005 | 0.3052 | 0.3177 |
| 0.5 | 0.4743 | 0.4954 | 0.5004 | 0.4997 | 0.5041 | 0.5239 |
| 0.8 | 0.7657 | 0.7797 | 0.7856 | 0.7865 | 0.7937 | 0.8239 |

Table 1: Summary of statistics for estimated roughness index $\widehat{H}_{L,K}$ from 150 independent simulations of fBm with $L = 300 \times 300$ and $K = 300$.

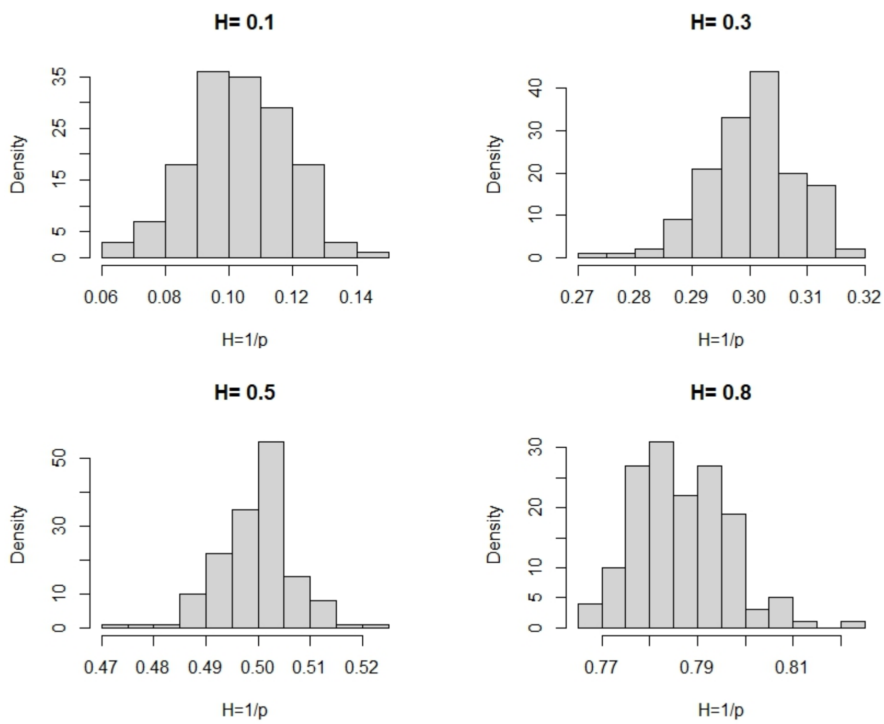


Figure 2: Histogram of estimated roughness index $\widehat{H}_{L,K}$ with $L = 300 \times 300$ and $K = 300$ generated from 150 independent simulation of fractional Brownian motions with Hurst parameter $H = \{0.1, 0.3, 0.5, 0.8\}$.

results are presented in Figure 3. Table 2 provides the summary statistics for the estimated roughness index $\widehat{H}_{L,K}$ corresponding to the histogram in Figure 3. We observe that the results are similar to those we obtained for $L = 300 \times 300$ and $K = 300$ but that the estimated roughness index $\hat{H}_{L,K}$ seems to be even more accurate. This is not surprising since we know that the normalized $p$-th variation statistic converges to the normalized $p$-th variation as $L$ and $K$ increase. However, increasing $L$ and $K$ is also computationally more demanding. The accuracy of $\widehat{H}_{L,K}$ obtained when using $L = 300 \times 300$ and $K = 300$ is also satisfactory for many purposes in this thesis.

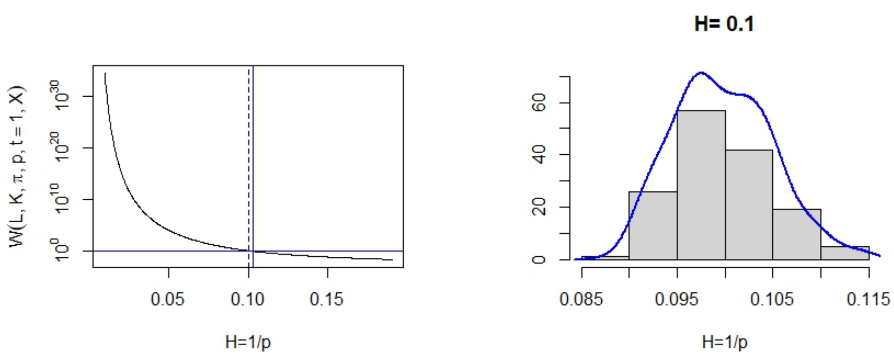


Figure 3: Simulation results for fractional Brownian motion with Hurst parameter $H = 0.1$. **Left:** The value of $\log(W(L = 2000 \times 2000, K = 2000, \pi, p, t = 1, X = B^H))$ plotted against $H = 1/p$ in black. The blue vertical line represents the estimated roughness $\hat{H}_{L,K}$ using $L = 2000 \times 2000$ and $K = 2000$. The vertical black dotted line represents the true Hurst parameter. **Right:** Histogram of estimated roughness index $\widehat{H}_{L,K}$ using $L = 2000 \times 2000$ and $K = 2000$ generated by 150 independent simulations of fBm with Hurst parameter $H = 0.1$. The blue line represents a kernel estimator for density.

| H | Min. | Lower quartile | Median | Mean | Upper quartile | Max. |
|---|---|---|---|---|---|---|
| 0.1 | 0.0892 | 0.0963 | 0.0996 | 0.0998 | 0.1031 | 0.1145 |

Table 2: Summary of statistics for estimated roughness index $\widehat{H}_{L,K}$ from 150 independent simulations of fBm with $H = 0.1$, $L = 2000 \times 2000$ and $K = 2000$.

We further investigate how the choice of $K << L$ affects the estimated roughness index $\hat{H}_{L,K}$. In Figure 4, we have plotted the estimated roughness $\hat{H}_{300\times 300,K}$ for a fractional Brownian motion with Hurst parameter $H = 0.1$ for different values of $K$ with a fixed $L = 300 \times 300$. Note that when $\frac{L}{K}$ is not an integer, the $K$ many groups from the definition of normalized $p$-th variation statistic (8) do not contain exactly $\frac{L}{K}$ consecutive points. The code is implemented such that each group will contain either $\lceil \frac{L}{K} \rceil$ or $\lfloor \frac{L}{K} \rfloor$ consecutive points. Figure 4 shows that when $K$ is too low, the estimator $\hat{H}_{300\times 300,K}$ seems to be underestimating the true Hurst parameter whereas when $K$ is too high the Hurst parameter is overestimated. For $K \approx \sqrt{L}$ the estimated roughness index is quite consistent and close to the true Hurst parameter $H = 0.1$. It is thus natural to use $K = \sqrt{L}$ since $\frac{L}{K}$ will be an integer and the estimator $\widehat{H}_{L,K}$ seems to be accurate and consistent in that range.

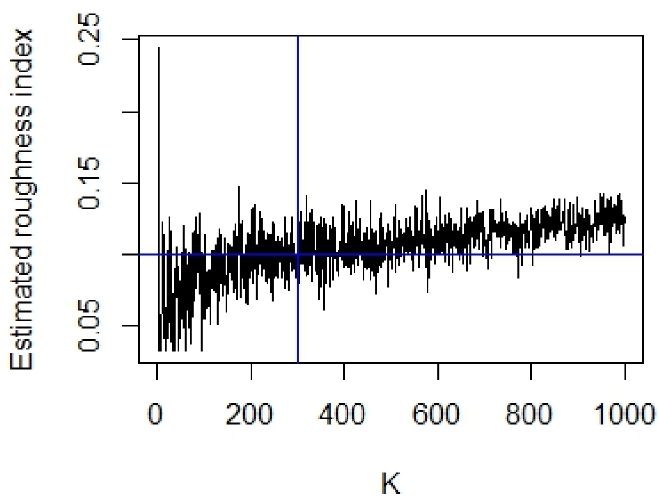


Figure 4: The solid black line represents the estimated roughness index $\hat{H}_{300\times 300,K}$ plotted against different values of $K$ for a simulation from a fBm with Hurst parameter $H = 0.1$. The blue vertical line represents $K = \sqrt{L} = 300$ whereas the blue horizontal line represents the true Hurst parameter $H = 0.1$.

In summary, these simulation examples show that for realistic sample sizes and frequencies encountered in high-frequency financial data, the roughness estimator via $p$-th variation $\widehat{H}_{L,K}$ is quite accurate and not sensitive to the block size $K$ in the range $K \approx \sqrt{L}$.

### 3.3 Roughness estimator via logarithmic regression

In this section we will introduce the roughness estimator via logarithmic regression used by Gatheral et al. [2018]. Following Gatheral et al. [2018] we consider a daily volatility process on the time interval $[0, T]$. First we pretend that we have access to discrete observations of the spot volatility process on a time grid with mesh size $\Delta$. That is, we pretend to have observations of the spot volatility at all points of the uniform time grid

$$\pi^n = (0 < \Delta < 2\Delta < ... < T)$$

such that the observations are $\sigma_0, \sigma_\Delta, ..., \sigma_{k\Delta}, ...$ for $k \in \{0, \lfloor T/\Delta \rfloor\}$. Let the total number of observation be $N = \lfloor T/\Delta \rfloor$. Then for $q \geq 0$ we define

$$m(q, \Delta) = \frac{1}{N} \sum_{k=1}^{N} |\log(\sigma_{k\Delta}) - \log(\sigma_{(k-1)\Delta})|^q.$$

Following Gatheral et al. [2018] the main assumption is that for some $s_q > 0$ and $b_q > 0$

$$N^{qs_q} m(q, \Delta) \to b_q \tag{10}$$

as $\Delta$ tends to zero. Under additional technical assumptions, this essentially means that the volatility process belongs to a Besov smoothness space $\mathcal{B}^{s_q}_{q,\infty}$ and does not belong to $\mathcal{B}^{s'_q}_{q,\infty}$ for $s'_q > s_q$. Hence, $s_q$ can be considered as a roughness parameter. In particular, functions in $\mathcal{B}^{s_q}_{q,\infty}$ for every $q > 0$ enjoy the Hölder condition of order $h$ for any $h < s_q$. For example if $\log(\sigma_t)$ is a fractional Brownian motion with Hurst parameter $H$, then for any $q \geq 0$ (10) holds in probability with $s_q = H$. It can further be shown that the sample paths of the process do indeed belong to $\mathcal{B}^{s_q}_{q,\infty}$. Thus, $s_q$ is a measure of roughness of the volatility process Gatheral et al. [2018].

The instantaneous volatility cannot be directly observed, and exact computations of $m(q, \Delta)$ is not possible in practice. In order to make use of $m(q, \Delta)$ we must therefore approximate the true spot volatility. The estimated volatility will be computed by the realized volatility or some variation of realized volatility. In the following we will be using the notation $m(q, \Delta)$ with the understanding that we are only approximating the true spot volatility, and $m(q, \Delta)$ will as such be based on discrete proxy values $\hat{\sigma}_{k\Delta}$ of spot volatility.
To estimate the roughness parameter $s_q$ for each $q$, we can compute $m(q, \Delta)$ for different values of $\Delta$ and regress $\log m(q, \Delta)$ against $\log \Delta$. Gatheral et al. [2018] only consider daily volatility estimates, and therefore the minimal value of $\Delta$ is $\Delta = 1$. Increasing $\Delta$ to $\Delta = 2$ then means that we are only using the daily volatility estimates for every second day and so forth.
Note that for a given $\Delta$ several $m(q, \Delta)$ can be computed depending on the starting point. For example, if $\Delta = 3$ then the starting point can be $\hat{\sigma}_0$, $\hat{\sigma}_\Delta$ or $\hat{\sigma}_{2\Delta}$. The final measure of $m(q, \Delta)$ is computed as the average of these values of $m(q, \Delta)$ with different starting points.

Gatheral et al. [2018] show that for a given $q$, $\log m(q, \Delta)$ values regressed against $\log \Delta$ essentially lie on a straight line. Assuming stationary increments of the log-volatility, this implies that the increments fulfil the scaling property

$$\mathbb{E}\left[|\log(\sigma_\Delta) - \log(\sigma_0)|^q\right] = b_q \Delta^{\zeta_q}$$

where $\zeta_q = q s_q > 0$ is the slope of the line associated to $q$. Note that $m(q, \Delta)$ can be seen as the empirical counterpart of $\mathbb{E}\left[|\log(\sigma_\Delta) - \log(\sigma_0)|^q\right]$. Furthermore, Gatheral et al. [2018] shows that $s_q$ seems to not depend on $q$, and plotting $\zeta_q$ against $q$ shows $\zeta_q \sim q s_q$.

Thus, we can compute an estimate of the roughness of a volatility process by first regressing $\log m(q, \Delta)$ against $\log \Delta$ for different values of $q$. The slope of the straight line is an estimate of $\zeta_q$. Next, we regress $\zeta_q$ against $q$. The slope of the straight line is an estimate of the roughness parameter $s_q$. If $\log(\sigma_t)$ is a fractional Brownian motion then $s_q = H$ holds in probability where $H$ is the Hurst parameter. We will let $\widehat{H}_R = s_q$ be the estimated roughness parameter by this procedure and refer to $\widehat{H}_R$ as the roughness estimator via log regression.

Note that with the above approach we are actually estimating the roughness of log-volatility. It is therefore implicitly assumed that log-volatility itself follows a model for which it makes sense to estimate roughness. If that is not the case, we would have to make modifications to the roughness estimator in order to make a sensible estimate.
For the numerical experiments we will perform in Section 4 we will not only consider daily volatility estimates. For some simulations we will set $T = 1$ and have many volatility observations per day. In order to retain the same notation and understanding of $\Delta$ we will elaborate on this setup. Let $a$ be the number of observations per day. For a given $\Delta$ we then consider the time grid with mesh size $a^{-1}\Delta$:

$$\pi^n = \left(0 < a^{-1}\Delta < 2a^{-1}\Delta < \ldots < T\right).$$

We then let $N = \lfloor \frac{T}{a^{-1}\Delta} \rfloor$ and for $q \geq 0$ we have

$$m(q, \Delta) = \frac{1}{N} \sum_{k=1}^{N} |\log(\sigma_{k a^{-1}\Delta}) - \log(\sigma_{(k-1)a^{-1}\Delta})|^q.$$

Thus, the meaning of $\Delta = 2$ is that we are only using every second observation of the time grid with mesh size $a^{-1}$, and we will still only be considering $\Delta \geq 1$. With this approach the results and plots in the numerical experiments can easily be compared to the case of daily volatility estimates.

In Figure 5 we have used the roughness estimator via log regression to replicate the roughness estimate from Gatheral et al. [2018] of volatility of S&P500 using the first 3500 days of the daily realized variance estimates from the Oxford-Man Institute of Quantitative Finance Realized Library for S&P. We have used $q = 0.5, 1, 1.5, 2, 3$ and $\Delta = 1, \ldots, 50$ for the estimation. Our results coincide with the results from Gatheral et al. [2018]. We find that $\log m(q, \Delta)$ values regressed against $\log \Delta$ lies on a straight line for all our values of $q$. Furthermore, $\zeta_q = q s_q$ plotted against $q$ also lie on a straight line. Our estimated roughness of the S&P realized volatility data is $\widehat{H}_R = 0.1421$.

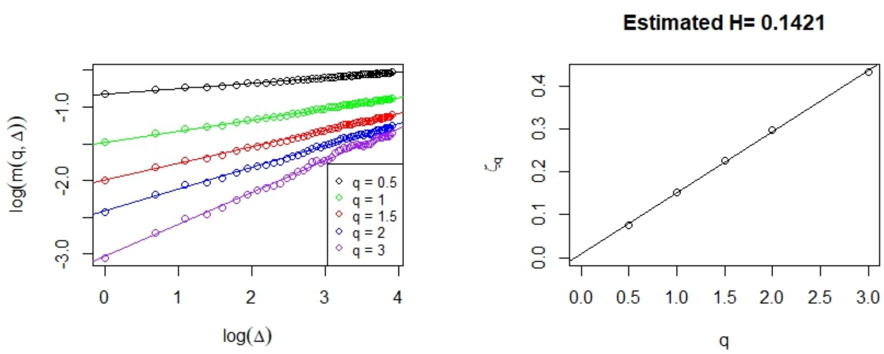


Figure 5: Roughness estimate via log regression of the first 3500 days of the daily realized volatility estimates from the Oxford-Man Institute of Quantitative Finance Realized Library for S&P. The estimated roughness is $\widehat{H}_R = 0.1421$.

Gatheral et al. [2018] perform roughness estimation similar to Figure 5 for other indices in the Oxford-Man dataset as well, and they systematically find that $m(q, \Delta)$ present a universal scaling behaviour. For the most common indices Gatheral et al. [2018] estimate the roughness of volatility $\widehat{H}_R$ in the range $[0.1, 0.15]$. Based on these results they propose a rough volatility model with $H < \frac{1}{2}$ and Gatheral et al. [2018] report $H = 0.14$ to be consistent with their empirical estimates.

In Figure 6 we have used the roughness index estimator via $p$-th variation from Section 3.2 on the same S&P volatility data used in Figure 5. We have used $W(L = 3500, K = \sqrt{3500}, \pi, p, t = 1, X)$ since the dataset only consist of 3500 days. We have set $t = 1$ and $T = 1$ in (9) for simplicity since $t$ simply works as a scaling parameter for $W(L, K, \pi, p, t, X)$ given that the same number of observations is used in the computations. The estimated roughness index is $\widehat{H}_{L,K} = 0.1425$. We immediately observe that the estimated roughness index is very close to the estimated roughness via log regression $\widehat{H}_R = 0.1421$. However, note that $L = 3500$ is much smaller than $L = 300 \times 300 = 90000$ for which we have investigated the accuracy of the roughness index estimator via $p$-th variation. Therefore, the estimated roughness estimator $\widehat{H}_{L,K}$ might not be very precise. The results do however indicate that our two different approaches to estimate the roughness of a volatility process coincides.

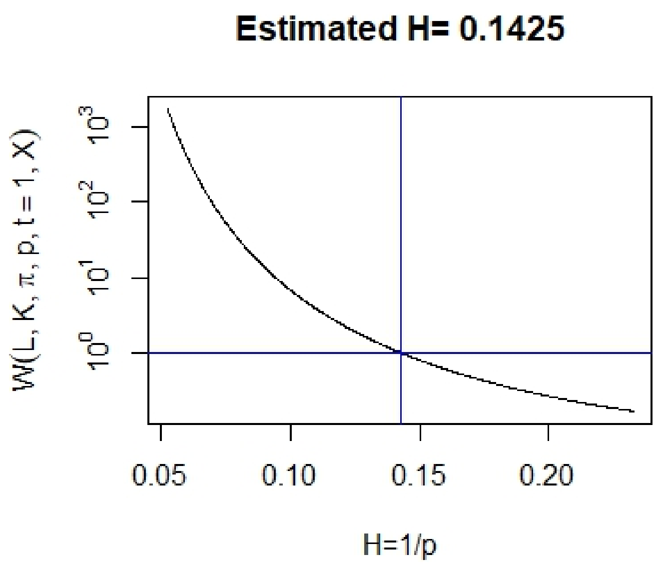


Figure 6: Estimating the roughness of the first 3500 days of S&P500 volatility data from Oxford-Man Institute of Quantitative Finance Realized Library using the roughness estimator from section 3.1 with $L = 3500$ and $K = \sqrt{3500}$. The estimated roughness index is $\hat{H}_{L,K} = 0.1425$.

### 3.4 The sequential scale estimator

The third estimator we will introduce, is the sequential scale estimator first introduced by Han and Schied [2023]. This estimator differs from many other roughness estimators by the fact that it is computed from discrete observations of cumulative integrated variance. Integrated variance is as in (5) given by

$$\langle logS \rangle_t = \int_0^t \sigma_s^2 ds.$$

The main reason for estimating roughness from integrated variance rather than from volatility estimates, is that integrated variance can quite accurately be computed from prices without first having to compute proxy values for volatility $\sigma_t$. As many roughness estimators in literature, the two previously described estimators are based on having access to discrete observations of instantaneous volatility $\sigma_t$. Realized volatility is then used as an approximation of the true spot volatility. This two step approach can be problematic since the estimation error in the realized volatility might substantially distort the outcome of the final roughness estimation. The sequential scale estimator is constructed with the purpose of avoiding this distortion caused by numerical errors in the computation of proxy values Han and Schied [2023].

Han and Schied [2023] are mainly concerned with stochastic volatility models based on fractional Brownian motions, but many aspects of the approach works in a model-free setting. Let $x : [0,1] \to \mathbb{R}$ be any continuous function. For $p \geq 1$ the $p$-th variation of the function $x$ along the $n$-th dyadic partition is defined as

$$\langle x \rangle_n^{(p)} := \sum_{k=0}^{2^n-1} |x((k+1)2^{-n}) - x(k2^{-n})|^p.$$

If there exist a $R \in [0,1]$ such that

$$\lim_{n\to\infty} \langle x \rangle_n^{(p)} = \begin{cases} 0 & \text{for } p > \frac{1}{R} \\ \infty & \text{for } p < \frac{1}{R} \end{cases}$$

we refer to $R$ as the roughness exponent of $x$. The smaller $R$ the rougher is the path $x$ and vice verse. Moreover, if $x$ is a sample path of a fractional Brownian motion, the roughness exponent R is equal to the Hurst parameter $H$ Han and Schied [2023]. Note that this roughness exponent is similar to the definition of roughness index from Definition 4.

Now, since only asset prices and their realized variance can be observed in practice, we can consider this as making discrete observations of

$$y(t) = \int_0^t g\left(x(s)\right) ds, \quad 0 \leq t \leq 1, \tag{11}$$

where $g : \mathbb{R} \to \mathbb{R}$ is sufficiently regular. Here $y(t)$ shall be seen as integrated variance and $g(x(t))$ as the variance of the process. For instance, if log-volatility is given by a fractional Ornstein-Uhlenbeck process, we will take $x$ as a sample path of a fractional Ornstein-Uhlenbeck process and $g(t) = (e^t)^2 = e^{2t}$.

For the sequential scale estimator, it is supposed that for a given $n \in \mathbb{N}$ we have access to the equidistant discrete observations $\{y(k2^{-n-2}) : k = 0, ..., 2^{n+2}\}$ of the integrated variance (i.e. the function $y$ in (11)). Based on these data points, the following coefficients are introduced

$$\vartheta_{n,k} := 2^{3n/2+3}\left(y\left(\frac{4k}{2^{n+2}}\right) - 2y\left(\frac{4k+1}{2^{n+2}}\right) + 2y\left(\frac{4k+3}{2^{n+2}}\right) - y\left(\frac{4k+4}{2^{n+2}}\right)\right),$$

for $0 \leq k \leq 2^n - 1$. The original scale estimator for the roughness exponent is then given by

$$\hat{\mathscr{R}}_n(y) := 1 - \frac{1}{n}\log_2\sqrt{\sum_{k=0}^{2^n-1}\vartheta_{n,k}^2}.$$

Detailed explanation of the rationale behind the estimator can be seen in Han and Schied [2022b]. Han and Schied [2023] show strong consistency results of $\hat{\mathscr{R}}_n$ when applied to typical trajectories of a fractional Brownian motion with possible drift or a rough Bergomi model.

The estimator $\hat{\mathscr{R}}_n(y)$ is not scale-invariant, and Han and Schied [2023] suggest to do scale-invariant modifications of $\hat{\mathscr{R}}_n(y)$. Fix $m \in \mathbb{N}$ with $n > m$ and fix $\alpha_0, ..., \alpha_m \geq 0$ with $\alpha_0 > 0$. The sequential scaling factor $\lambda_n^s$ is then defined as

$$\lambda_n^s := \arg\min_{\lambda>0}\sum_{k=n-m}^{n}\alpha_{n-k}\left(\hat{\mathscr{R}}_k(\lambda y) - \hat{\mathscr{R}}_{k-1}(\lambda y)\right)^2. \tag{12}$$

The sequential scale estimate $\hat{\mathscr{R}}_n^s(y)$ is then defined as follows

$$\hat{\mathscr{R}}_n^s(y) := \hat{\mathscr{R}}_n(\lambda_n^s y).$$

The idea is that the sequential scaling factor $\lambda_n^s$ enforces the convergence of $\hat{\mathscr{R}}_n(\lambda_n^s y)$. Thus, $\hat{\mathscr{R}}_n^s(y)$ will in some cases converge faster than $\hat{\mathscr{R}}_n(y)$ and remove bias. Han and Schied [2023] prove that the sequential scale estimator is scale-invariant and has a unique solution for every function $y \in C[0, 1]$.

### 3.4.1 Sequential scale estimate from realized variance

In practice integrated variance (5) is not observable and needs to be approximated. It is usually approximated by realized variance That is, realized variance (4) which is computed from discrete observations of $S_t$ is used as an approximation of integrated variance. The error between integrated and realized variance has been studied in Bolko et al. [2023] and Fukasawa et al. [2022]. The error arising from the approximation often results in a underestimation of the roughness exponent of the hidden volatility process $\sigma_t$. However, Han and Schied [2023] argue that the sequential scale estimator is effective in accommodating the proxy error. We will now describe the sequential scale estimation when based directly on realized variance.

We will denote the integrated variance by

$$Y_t = \langle logS \rangle_t = \int_0^t \sigma_s^2 ds, \quad 0 \leq t \leq 1.$$

Let $(m_n)_{n \in \mathbb{N}_0}$ be a fixed increasing sequence, where $m_n$ can be regarded as the number of observed data points used to compute the realized variance over each interval $[k2^{-n}, (k+1)2^{-n}]$. Then we can denote the realized variance in this setting as

$$\widehat{Y}_t^{(n)} := \sum_{k=1}^{\lfloor 2^n m_n t \rfloor} \left( \log S_{\frac{k}{2^n m_n}} - \log S_{\frac{k-1}{2^n m_n}} \right)^2. \tag{13}$$

Thus, the process $\widehat{Y}_t^{(n)}$ is the realized variance calculated from the price process $S_t$ with a mesh size $(2^n m_n)^{-1}$. From $\widehat{Y}_t^{(n)}$ we can define the proxy coefficients $\widetilde{\vartheta}_{n,k}$ as

$$\widetilde{\vartheta}_{n,k} := 2^{3n/2+3} \left( \widehat{Y}^{(n+2)}_{\frac{4k}{2^{n+2}}} - 2\widehat{Y}^{(n+2)}_{\frac{4k+1}{2^{n+2}}} + 2\widehat{Y}^{(n+2)}_{\frac{4k+3}{2^{n+2}}} - \widehat{Y}^{(n+2)}_{\frac{4k+4}{2^{n+2}}} \right).$$

By replacing $\vartheta_{n,k}$ with $\widetilde{\vartheta}_{n,k}$ we can construct an estimator $\widetilde{\mathscr{R}}_n(y)$ that directly estimates the roughness exponent from the realized variance as follows

$$\widetilde{\mathscr{R}}_n(S) := 1 - \frac{1}{n} \log_2 \sqrt{\sum_{k=0}^{2^n-1} \widetilde{\vartheta}^2_{n,k}}$$

where $S$ denotes the price process that $\widetilde{\mathscr{R}}_n$ estimates from.

To incorporate the proxy error into the framework Han and Schied [2023] make an assumption on the difference between $\widehat{Y}_t^{(n)}$ and $Y_t$. Let

$$Z_k^{(n)} := \left( \widehat{Y}^{(n)}_{\frac{k}{2^n}} - \widehat{Y}^{(n)}_{\frac{k-1}{2^n}} \right) - \left( Y_{\frac{k}{2^n}} - Y_{\frac{k-1}{2^n}} \right).$$

Furthermore, let $\mathscr{F}^\sigma = \bigcup_{t \geq 0} \mathscr{F}_t^\sigma$ where $\mathscr{F}_t^\sigma = \sigma(\{\sigma_s, s \in [0,t]\})$.

**Assumption 1.** *The random variables* $\left( Z_k^{(n)} \right)$ *are independent conditionally on* $\mathscr{F}^\sigma$ *and*

$$Z_k^{(n)} | \mathscr{F}^\sigma \sim \mathcal{N} \left( 0, \frac{2}{2^n m_n} \int_{\frac{k-1}{2^n}}^{\frac{k}{2^n}} \sigma_s^4 ds \right).$$

*Furthermore, it is assumed that* $\mathbb{E}[\int_0^1 \sigma_s^8 ds] < \infty$.

Under this assumption the following theorem holds which states that $\hat{\mathscr{R}}_n(Y)$ and $\widetilde{\mathscr{R}}_n(S)$ converge to the same limit given that $m_n$ grows fast enough.

**Theorem 1.** *Suppose that Assumption 1 holds and there exist* $R \in (0,1)$ *such that* $\hat{\mathscr{R}}_n(Y) \to R$ *almost surely. If*

$$\lim_{n \uparrow \infty} \frac{1}{n} \log_2 m_n > 2R.$$

*then* $\widetilde{\mathscr{R}}_n(S) \to R$ *with probability one as* $n$ *increases.*

The proof of Theorem 1 can be seen in Han and Schied [2023]. The result specifies the number of data points $m_n$ required to compute realized variance in each interval in order for $\widetilde{\mathscr{R}}_n$ to be a consistent estimator. Particularly, we see that if the volatility process is smooth (i.e. $R > \frac{1}{2}$) more points are required in each realized variance computation in order to have consistency compared to a rough process.

In the sequel it will be clear that $\hat{\mathscr{R}}_n^s$ can significantly improve $\hat{\mathscr{R}}_n$. We will by $\widetilde{\mathscr{R}}_n^s(S)$ denote the sequential scale estimator of realized variance which is defined as

$$\widetilde{\mathscr{R}}_n^s(\widehat{Y}_t^{(n)}) := \widetilde{\mathscr{R}}_n(\lambda_n^s \widehat{Y}_t^{(n)})$$

where $\lambda_n^s$ is computed in the same manner as (12) just using $\widetilde{\mathscr{R}}_n(\widehat{Y}_t^{(n)})$ instead of $\widehat{\mathscr{R}}_n(Y)$. However, Han and Schied [2023] does not discuss consistency of $\widetilde{\mathscr{R}}_n^s(S)$.

#### 3.4.2 Sample behaviour of $\hat{\mathscr{R}}_n^s$ and $\hat{\mathscr{R}}_n$

We will now illustrate the performance of $\hat{\mathscr{R}}_n^s(y)$ and $\hat{\mathscr{R}}_n(y)$ in a simple examples by replicating the simulation examples from Han and Schied [2023].

First, we let $x$ follow a sample path of a fractional Brownian motion $B_t^H$ and set $g(x) = x$. For the computation of $\hat{\mathscr{R}}_n(y)$ we require observations of $y$ at all values of the time grid $\mathbb{T}_{n+2} := \{k2^{-n-2} : k = 0, 1, ..., 2^{n+2}\}$. In order to approximate $y(t) = \int_0^t B_s^H ds$ we are simulating the values of $B_t^H$ on a finer time grid $\mathbb{T}_N$ with $N = n + 6$. Then we put

$$Y_{k2^{-n-2}} := 2^{-N} \sum_{j=1}^{2^{N-n-2}k} B^H_{j2^{-N}}, \quad k = 0, 1, ..., 2^{n+2} \tag{14}$$

which is an approximation of $y(t) = \int_0^t B_s^H ds$ by Riemann sums. In Figure 7 we display the results for the estimators $\hat{\mathscr{R}}_n$ and $\hat{\mathscr{R}}_n^s$ for 1000 independent paths of a fractional Brownian motion for different values of $n$. The left plot of Figure 7 is based on paths from a fractional Brownian motion with Hurst exponent $H = 0.3$ while the right plot is for a fBm with $H = 0.7$. The top plots are from the original estimator $\hat{\mathscr{R}}_n$ whereas the bottom plots are box plots of the sequential scale estimates $\hat{\mathscr{R}}^s_n$. We observe from the top plots in Figure 7 that $\hat{\mathscr{R}}_n$ performs relatively well and seems to converge to the true roughness exponent as $n$ increases. However, the estimator also exhibits a certain bias. The corresponding results for the sequential scale estimator $\hat{\mathscr{R}}^s_n$ are displayed in the bottom plots of Figure 7. We observe that by passing to the sequential scale estimator we completely remove the bias observed for $\hat{\mathscr{R}}_n$. Overall, $\hat{\mathscr{R}}^s_n$ seems to be a quite accurate estimate especially for $n \geq 15$.

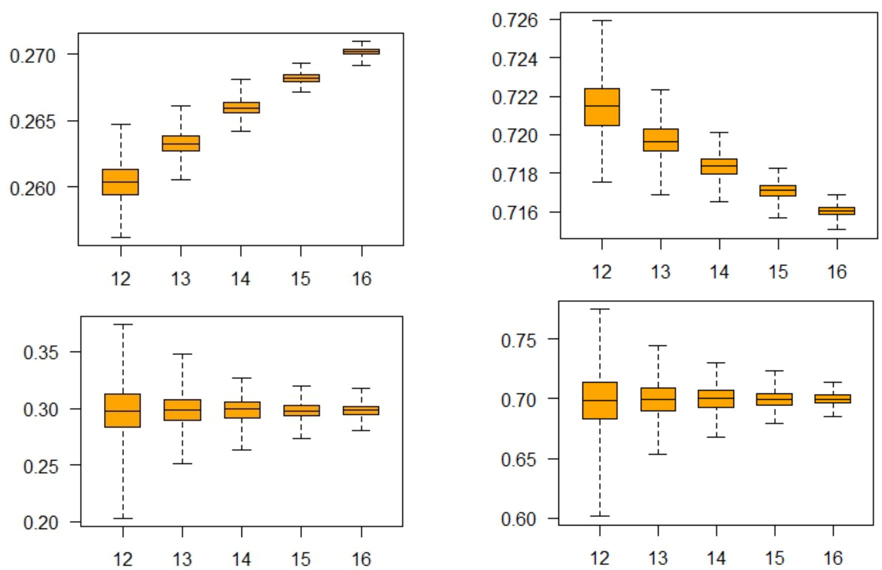


Figure 7: Box plots of the original estimates $\hat{\mathscr{R}}_n(Y)$ (top) and the sequential scale estimates $\hat{\mathscr{R}}^s_n(Y)$ (bottom) for $n = 12, ..., 16$ based on 1000 independent simulations of a fractional Brownian motion with $H = 0.3$ (left) and $H = 0.7$ (right) and with $Y$ as in (14). The other parameters are chosen to be $m = 3$ and $\alpha_k = 1$ for $k = 0, 1, 2, 3$.

We now make a bit more complicated simulation example. We let log volatility, $\log \sigma_t$ be given by a fractional Ornstein-Uhlenbeck process on the form

$$dX_t = +\rho(\mu - X_t)\,dt + dB^H_t \tag{15}$$

where $B^H_t$ is a fractional Brownian motion. In this example we use the parameters $\rho = 0.2$, $X_0 = 0$ and $\mu = 2$. As input to the estimator we need discrete observations of

$$\int_0^t \sigma_s^2 ds = \int_0^t e^{2X_s} ds, \quad 0 \leq t \leq 1.$$

To this end, we take again $N = n + 6$ and simulate the values of $X_t$ on the finer time grid $\mathbb{T}_N := \{k2^{-N} : k = 0, 1, ..., 2^N\}$ by an Euler scheme. We then compute

$$Y_{k2^{-n-2}} := 2^{-N} \sum_{j=1}^{2^{N-n-2}k} exp\left(2X_{j2^{-N}}\right), \quad k = 0, 1, ..., 2^{n+2} \tag{16}$$

as an approximation of $\int_0^t e^{2X_s} ds$. In Figure 8 we display the results for the estimators $\hat{\mathscr{R}}_n$ and $\hat{\mathscr{R}}_n^s$ for 1000 independent paths of (15) with $n = 12, ..., 16$. The left plot of Figure 8 is based on paths from a Ornstein-Uhlenbeck process with Hurst exponent $H = 0.3$ while the right plot is for a fOU with $H = 0.7$. The top plots are from the original estimator $\hat{\mathscr{R}}_n$ whereas the bottom plots are box plots of the sequential scale estimates $\hat{\mathscr{R}}_n^s$. We observe from the top plots in Figure 7 that the original estimator $\hat{\mathscr{R}}_n$ performs poorly in this case. However, the sequential scale estimator $\hat{\mathscr{R}}_n^s$ performs almost as well as in the simple case illustrated in Figure 7. This is likely due to the fact that $g(t) = e^{2t}$ used in (16) substantially distort the scale of the underlying process. Since the original estimator is not scale-invariant this leads to poor estimates. However, passing to $\hat{\mathscr{R}}_n^s(y)$ seems to completely remedy this distortion.

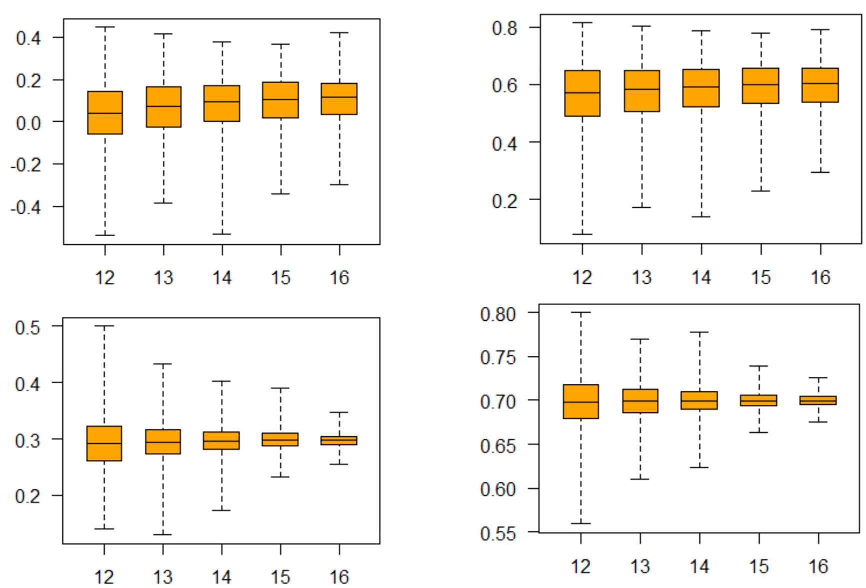


Figure 8: Box plots of the original estimates $\hat{\mathscr{R}}_n(Y)$ (top) and the sequential scale estimates $\hat{\mathscr{R}}_n^s(Y)$ (bottom) for $n = 12, ..., 16$ based on 1000 independent simulations of a fractional Ornstein-Uhlenbeck process (15) with $H = 0.3$ (left) and $H = 0.7$ (right) and with $Y$ as in (16). The other parameters are chosen to be $m = 3$ and $\alpha_k = 1$ for $k = 0, 1, 2, 3$.

Both of these simulation examples illustrate how the sequential scale estimator $\widehat{\mathscr{R}}^s_n$ improves the estimator $\widehat{\mathscr{R}}_n$. Overall, $\widehat{\mathscr{R}}^s_n$ seems to be performing very well and provide an accurate estimate of the true roughness of the underlying model especially for $n \geq 15$. We will be using the sequential scale estimator $\widehat{\mathscr{R}}^s_n$ and $\widetilde{\mathscr{R}}^s_n$, and the original scale estimator $\widehat{\mathscr{R}}_n$ and $\widetilde{\mathscr{R}}_n$ when performing numerical experiments in Section 4.

# 4 Numerical Experiments

In this section, we will be performing a number of numerical experiments. We will estimate the roughness of paths generated from stochastic models with various degrees of roughness by using our three introduced roughness estimators. The estimates will be computed for instantaneous volatility $\sigma_t$ and realized volatility by using price trajectories simulated from the models. By doing this we can investigate how estimation errors impact the estimated roughness. For the sequential scale estimator we will approximate integrated variance directly from instantaneous volatility, and compare these results to estimates obtained from realized variance.

## 4.1 Simple stochastic volatility diffusion model

First, we will consider the following stochastic volatility model where the volatility is the modulus of a Brownian motion:

$$dS_t = \sigma_t S_t dB_t \quad \text{with} \quad \sigma_t = |B'_t|, \tag{17}$$

where $S_t$ is the price of the asset and $B_t$ and $B'_t$ are two independent Brownian motions. For the simulations we use $S_0 = 1$ and $T = 1$, and we will simulate by an Euler scheme. The true roughness of this model is simply $H = 0.5$.

Following Cont and Das [2024] we will compute realized volatility using Definition 1 for 300 consecutive points which corresponds to a 5 minute moving window when the price is updated every second. We estimate the roughness of the realized volatility process and also of the instantaneous volatility process $\sigma_t$. We will rescale the computed realized volatility such that it work as a proxy value of instantaneous volatility $\sigma_t$. The corresponding instantaneous volatility we will be using, is the $\sigma_t$ for the first of these 300 consecutive points.

For this example, we will compute the roughness index estimator via $p$-th variation $\widehat{H}_{L,K}$ with $L = 500 \times 500$ and $K = 500$ of the volatility processes. Therefore, we will generate $300 \times 500 \times 500$ points in order to have $L$ observations of realized volatility.

In Figure 9, we have made plots for the realized and instantaneous volatility generated from model (17). The left plot of Figure 9 represents the realized volatility of the price process in black and the instantaneous volatility in red for the first 10000 observations of these. The middle plot of Figure 9 represents the difference between the realized and instantaneous volatility which is the estimation error. The right plot of Figure 9 represents the log difference which is computed as the difference between the log of realized volatility and the log of instantaneous volatility. Figure 9 indicates that instantaneous and realized volatility broadly correspond. However, there clearly exist an estimation error. The two right plots of Figure 9 indicate that the estimations error has a complicated dependence structure. There seems to be no obvious pattern in the estimation error and both the estimation error and log estimation error are far from I.I.D.

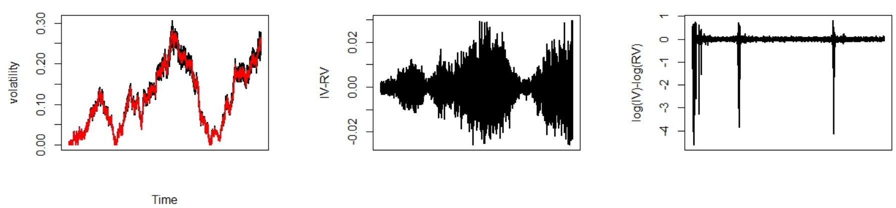


Figure 9: Simulation from model (17). **Left:** The red line represents instantaneous volatility $\sigma_t$ whereas the black line represents realized volatility $RV_t$. **Middle:** Corresponding estimation error for the left simulated path. **Right:** Corresponding log estimation error.

In Figure 10 we have estimated the roughness by the roughness index estimator via $p$-th variation from Section 3.2 for realized and instantaneous volatility respectively. In the left plot, we have used realized volatility as input to the normalized $p$-th variation statistic and plotted $\log(W(K = 500, L = 500 \times 500, \pi, p, t = 1, X = RV))$ against $H = \frac{1}{p}$. The right graph is a similar plot using instantaneous volatility instead of realized volatility. The obtained roughness estimators are very different for instantaneous and realized volatility. For realized volatility we obtain an estimated roughness of $\hat{H}_{L=500\times500,K=500}(RV) = 0.323$ which is much lower than the estimated roughness index for instantaneous volatility $\hat{H}_{L=500\times500,K=500}(\sigma) = 0.499$. The true roughness of the model is $H = 0.5$. Thus, the roughness estimator is quite accurate when using instantaneous volatility which is in accordance with our results from Section 3.2. However, the estimated roughness when using realized volatility is much rougher than the true roughness of the model. As this is a simulation study we do have any measurement errors, and this rougher behaviour of realized volatility purely comes from the estimation error.

In Figure 11 we have plotted the estimated roughness index $\widehat{H}_{L=500\times500,K}$ against different values of $K$. The left graph is for realized volatility while the right graph is for instantaneous volatility. The blue lines represents the

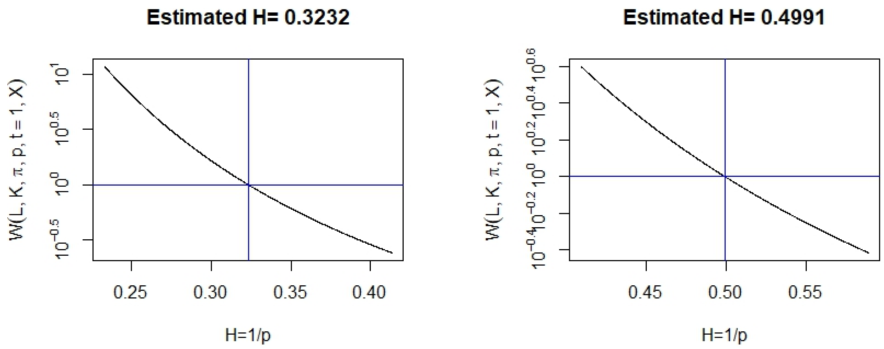


Figure 10: The value of $\log(W(L = 500 \times 500, K = 500, \pi, p, t = 1, X))$ plotted against $H = 1/p$ in black. The blue vertical line represents the estimated roughness $\hat{H}_{L,K}$. **Left:** Estimated roughness index $\hat{H}_{L,K}$ for realized volatility derived from the stochastic volatility model (17). **Right:** Estimated roughness index for instantaneous volatility of the same price path.

estimated roughness $\hat{H}_{L,K}$ with $L = 500 \times 500$ and $K = 500$ which are also reported in Figure 10. From the figure, we observe that irrespective of the choice of $K$ for the finite sample dataset of length $L = 500 \times 500$, the realized volatility is significantly rougher than the instantaneous volatility. The estimated roughness of the volatilities are quite consistent as long as $K$ is not too low for both volatilities. However, $\widehat{H}_{L=500\times500,K}$ seems to be even more consistent for instantaneous volatility than for realized volatility.

We now want to use the sequential scale estimator $\widehat{\mathscr{R}}^s_n$ for this example. We wish to estimate the roughness for the same path that Figure 10 was based on. The sequential scale estimator requires observations of integrated variance $y(t) = \int_0^t g(x(s))\, ds$ at all values of the time grid $\mathbb{T}_{n+2} := \{k2^{-n-2} : k = 0, 1, ..., 2^{n+2}\}$. To accommodate for that we rescale our simulated path from before such that we have observations at the required time points. In the spirit of Theorem 1 we want to make sure that $m_n$ is sufficiently large in order to have consistency of $\widetilde{\mathscr{R}}^s_n$. We will choose $n = 12$ and $m_n = 2^{12}$ such that $\frac{1}{n}\log_2 m_n = 1$. Furthermore, we use the parameters $m = 4$ and $\alpha_k = 1$ for $k = 0, 1, 2, 3$ for the computation of $\widetilde{\mathscr{R}}^s_n$.
The number of data points in each interval $[k2^{-n}, (k+1)2^{-n}]$ is then $m_n = 2^{12}$. We now follow the procedure described in Section 3.4.1 to make a roughness estimate from realized variance. To this end, we need observations of the price process on the finer time grid $\mathbb{T}_N$ with $N = n + 14$. Therefore, we need $2^N + 1$ points on the time interval $t \in [0, 1]$.

Based on the sample behaviour of $\widehat{\mathscr{R}}^s_n$ in Section 3.4.2 it would be desirable to further increase $n$ to make the estimator more accurate. However, according

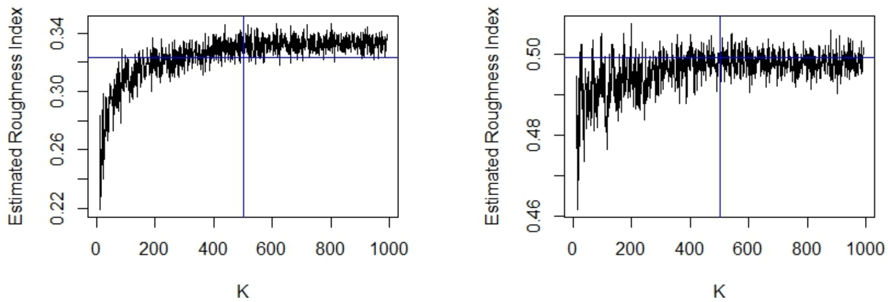


Figure 11: The value of the estimated roughness index $\hat{H}_{L=500\times500,K}$ plotted against different values of $K$. **Left:** Estimated roughness index $\hat{H}_{L=500\times500,K}$ for realized volatility derived from the stochastic volatility model (17). The horizontal blue line represents $\hat{H}_{L=500\times500,K=500} = 0.323$. **Right:** Estimated roughness index for instantaneous volatility of the same price path. The horizontal blue line represents $\hat{H}_{L=500\times500,K=500} = 0.499$.

to Theorem 1 we need $\lim_{n\uparrow\infty} \frac{1}{n}\log_2 m_n > 2H$ to make sure that proxy errors will not distort the roughness estimate from realized variance. Thus, to accommodate these two things we can maximally choose $n = 12$ and $m_n = 2^{12}$ given the number of observations we have generated. To further increase $n$ and $m_n$ we would need many more observations. Such a sample size and frequency seems highly unrealistic in practical applications. We will investigate the performance of $\widetilde{\mathscr{R}}^s_n$ for $n = 12$ and $m_n = 2^{12}$ for which we need $2^{26}$ observations on the time interval $t \in [0, 1]$.

For these new points for the sequential scale estimator we have a mesh size $\Delta t = (2^n m_n)^{-1} = 2^{-N}$. We rescale the first $2^N$ points of our simulated Brownian motions $B_t$ and $B'_t$ such that they correspond to this new $\Delta t$. We then generate the price process as in (17) using these rescaled Brownian motions. In Figure 12 we have plotted the first 100000 data points of the original price process $S_t$ on the left and the corresponding rescaled price process on the right. We observe that the prices processes follow the exact same pattern. The only difference between the graphs is the axes that have been rescaled since we have rescaled the whole prices process. Hence, we would expect the same roughness of volatility for these two price processes.

We then compute the realized variance as in (13). In order to investigate possible distortion caused by proxy errors of integrated variance we wish to compare realized variance with integrated variance. To this end, we also approximate

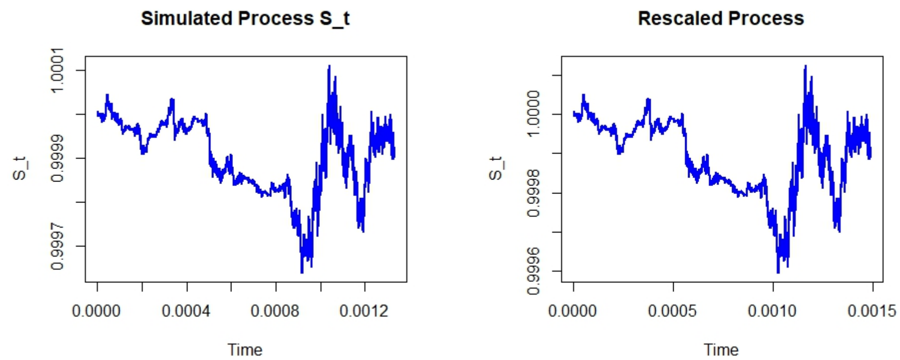


Figure 12: The first 100000 data points of the simulated price process $S_t$ generated from model (17). The left plot is the original simulated path while the right plot is the rescaled price process with slightly fewer points and a different mesh size used for the sequential scale estimator.

$y(t) = \int_0^t g\left(x(s)\right) ds$ directly from $\sigma_t$ by

$$Y_{k2^{-n-2}}(\sigma) = 2^{-N} \sum_{j=1}^{2^{N-n-2}k} \sigma^2_{j2^{-N}}, \quad k = 0, 1, ..., 2^{n+2} \tag{18}$$

which is an approximation of integrated variance by Riemann sums. In the following we will sometimes refer to $Y_t(\sigma)$ from (18) as integrated variance since the difference between integrated variance and $Y_t(\sigma)$ can be neglected in our examples.

In Figure 13 we have plotted these two approximations of integrated variance and their difference. The left plot of Figure 13 represent realized variance $\widehat{Y}_t^{(n)}$ in black and the approximation $Y_t(\sigma)$ directly from $\sigma_t$ as in (18) in red. The middle plot shows the difference between these two approximations of integrated variance, and the right plot shows the difference between the log of the two approximations. Figure 13 indicates that these two ways of computing the integrated variance yield very similar results, and the difference between realized variance and $Y_t(\sigma)$ is very small. On the left plot it is very difficult to distinguish the red and the black line from each other since they fall directly on top of each other. However, there is a very small difference as seen on the two plots to the right, and especially the log difference is somewhat big in the very beginning when the integrated variance is very small.

We now proceed to estimating the roughness by using respectively realized variance and integrated variance $Y_t(\sigma)$. We denote the sequential scale estimator based directly on realized variance by $\widetilde{\mathscr{R}}^s_n(S)$ whereas the roughness estimated

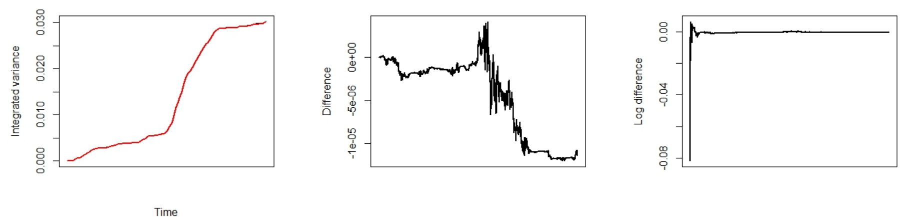


Figure 13: Integrated variance of the original path from model (17) rescaled to fit the sequential scale estimator. **Left:** The red line represents $Y$ computed directly from instantaneous volatility $\sigma_t$ whereas the black line represents realized variance $\hat{Y}_t^{(n)}$. **Middle:** Corresponding difference between the lines in the left plot. **Right:** Corresponding log difference.

from $Y(\sigma_t)$ is denoted by $\widehat{\mathscr{R}}^s_n(Y)$. Table 3 provides the roughness estimates obtained from the sequential scale estimator for the rescaled path from model (17). Furthermore, the table also provides the results from the original estimators $\widetilde{\mathscr{R}}_n(S)$ and $\widehat{\mathscr{R}}_n(Y)$ that are used for the computations of $\widetilde{\mathscr{R}}^s_n(S)$ and $\widehat{\mathscr{R}}^s_n(Y)$.

| | Realized variance | Integrated variance $Y_t(\sigma)$ |
|---|---|---|
| Sequential scale estimator | $\widetilde{\mathscr{R}}^s_n(S) = 0.2976$ | $\widehat{\mathscr{R}}^s_n(Y) = 0.4738$ |
| Original scale estimator | $\widetilde{\mathscr{R}}_n(S) = 0.4781$ | $\widehat{\mathscr{R}}_n(Y) = 0.5488$ |

Table 3: The roughness estimates from the sequential scale roughness estimator with $n = 12$ and $m_{12} = 2^{12}$ for model (17) by using respectively realized variance and the approximation of integrated variance from instantaneous volatility $Y_t(\sigma)$.

Even though the difference between realized variance $\widehat{Y}_t^{(n)}$ and $Y_t(\sigma)$ is small, the sequential scale estimator yields very different results when used for these two variances as seen in Table 3. The estimated roughness when using integrated variance based on instantaneous volatility $Y(\sigma_t)$ is near the true roughness of the model $H = \frac{1}{2}$. However, when using realized variance the estimated roughness is $\widetilde{\mathscr{R}}^s_n(S) = 0.2976$ which is much rougher than the true roughness of the model and close to the estimated roughness index for realized volatility from before $\hat{H}_{L=500\times 500, K=500} = 0.323$.
This indicates that the estimator $\widetilde{\mathscr{R}}^s_n(S)$ is also vulnerable to proxy errors where proxy errors in this case is difference between realized variance and integrated variance. It is clear that the proxy error is smaller for the sequential scale estimator in the sense that the difference between realized variance $\widehat{Y}_t^{(n)}$ and

$Y_t(\sigma)$ observed in Figure 13 is much smaller than the difference between realized volatility and instantaneous volatility observed in Figure 9.
However, the small difference between $\widehat{Y}_t^{(n)}$ and $Y_(\sigma)$ is enough to substantially distort the outcomes of the roughness estimation. Furthermore, we observe from Table 3 that the original estimator $\widetilde{\mathscr{R}}_n(S)$ actually performs better than the sequential scale estimator $\widetilde{\mathscr{R}}_n^s(S)$ when used for realized variance. This is not in accordance with our simulation results from Section 3.4.2 where we illustrated how passing to the sequential scale estimator could remove bias and make the estimator converge faster. However since we are using $n = 12$ we would expect some variation to the estimates and this might just be a matter of the individual path.

In Figure 14 we have repeated the estimation procedure across 150 independent paths drawn from model (17) and computed $\widehat{H}_{L,K}$, $\widetilde{\mathscr{R}}_n^s$ and $\widehat{\mathscr{R}}_n$ for all paths. The left plot of Figure 14 displays density plots of the estimators when used on realized volatility and realized variance whereas the right plot displays density plots when using instantaneous volatility and $Y_t(\sigma)$ as input to the estimators. For $\widehat{H}_{L,K}$ we observe that when using realized volatility the estimator $\widehat{H}_{L,K}(RV)$ systematically underestimates the true roughness exponent of $H = \frac{1}{2}$. However, when used on instantaneous volatility $\widehat{H}_{L,K}(IV)$ is very accurate and estimates the true roughness of the model very well.
Similar conclusions can be drawn for the sequential scale estimator $\widehat{\mathscr{R}}_n^s$. Although not as consistent as $\widehat{H}_{L,K}(IV)$ it seems to estimate the roughness from integrated variance decently, and it seems to be an unbiased estimator in that case. However, when input is realized variance $\widehat{Y}_t^{(n)}$, the estimator performs poorly and is far from unbiased. The estimates varies quite a lot, and the mean of $\widetilde{\mathscr{R}}_n^s(S)$ seems to be in the same range as $\widehat{H}_{L,K}(RV)$ meaning a significant underestimation of the true roughness of the volatility process.
Furthermore, we observe that the original scale estimator $\widetilde{\mathscr{R}}_n(S)$ actually yields more accurate results when estimating the roughness from realized variance. That is, passing to the sequential scale estimator adds more bias to the estimate in that case. This is unexpected since we would expect $\widetilde{\mathscr{R}}_n^s$ to improve the original estimator.

### 4.2 OU-SV model

Now, we will simulate from the following Ornstein-Uhlenbeck stochastic volatility model:

$$dS_t = S_t\sigma_t dB_t, \quad \sigma_t = \sigma_0 e^{Z_t}, \quad dZ_t = -\gamma Z_t\, dt + \theta\, dB'_t, \tag{19}$$

where $S_t$ is the price of the asset and $B_t$ and $B'_t$ are two independent Brownian motions. In the simulation, we are using the parameters $\sigma_0 = \gamma = \theta = 1$ and $Z_0 = 0$ and we set $T = 5$ and $S_0 = 1$. We will simulate by an Euler scheme.

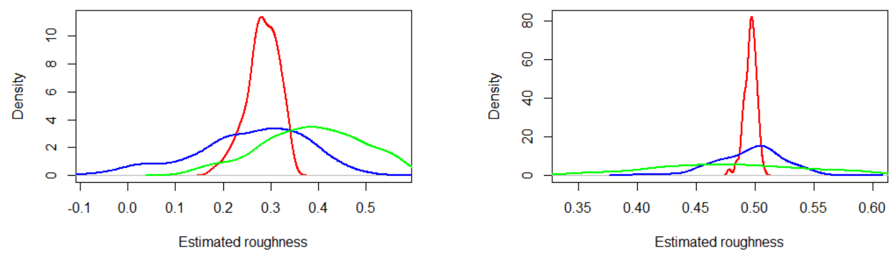


Figure 14: Density plots of the roughness estimators $\widehat{H}_{L,K}$ (red), $\widetilde{\mathscr{R}}^s_n(S)$ and $\widehat{\mathscr{R}}^s_n(Y)$ (blue), and $\widetilde{\mathscr{R}}_n(S)$ and $\widehat{\mathscr{R}}_n(Y)$ (green) across 150 independent paths drawn from model (17). **Left:** Using realized volatility and realized variance as input. **Right:** Using instantaneous volatility $\sigma_t$ and $Y_t(\sigma)$ as input.

The true roughness of this model is $H = 0.5$.

We are using the same procedure as described in Section 4.1 to generate our realized and instantaneous volatility. We will for this example use $L = 300 \times 300$ and $K = 300$. Therefore, we generate $300 \times L = 300 \times 300 \times 300$ simulated points from our model. In Figure 15, we have made plots for the volatilities. The left plot of Figure 15 represents the realized volatility of the price process in black and the instantaneous volatility in red. The middle plot of Figure 15 represents the difference between the realized and instantaneous volatility which is the estimation error. The right plot of Figure 15 represents the log difference between the realized and instantaneous volatility. Visually the middle plot suggests that the estimation error has a complicated dependence structure. However, the log estimation error on the right plot of Figure 15 seems to have an I.I.D. Gaussian structure. This is supported by the theory in Fukasawa et al. [2022]. However, as shown in Section 4.1 the I.I.D. behaviour of the log estimation error does not in general hold for stochastic diffusive models as assumed in Fukasawa et al. [2022].

In Figure 16 we have estimated the roughness index via normalized $p$-th variation for realized and instantaneous volatility. In the left plot, we have used the realized volatility as input to the normalized $p$-th variation statistic and plotted $\log(W(K = 300, L = 300 \times 300, \pi, p, t = 1, X = RV))$ against $H = \frac{1}{p}$. The right graph is a similar plot using instantaneous volatility instead of realized volatility. The obtained roughness estimators are very different for instantaneous and realized volatility. For realized volatility we obtain an estimated roughness of $\hat{H}_{L=300\times300,K=300}(RV) = 0.155$ which is much lower than the estimated roughness index for instantaneous volatility $\hat{H}_{L=300\times300,K=300}(\sigma) = 0.501$. The true roughness of the model is $H = 0.5$. Thus, also for this example the roughness

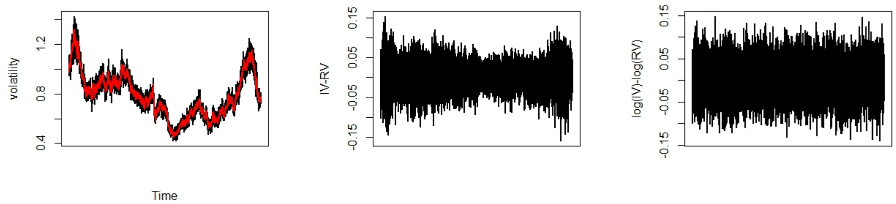


Figure 15: Simulation from the OU-SV model. **Left:** The red line represents instantaneous volatility $\sigma_t$ whereas the black line represents realized volatility $RV_t$. **Middle:** Corresponding estimation error for the left simulated path. **Right:** Corresponding log estimation error.

estimator is very accurate when using instantaneous volatility. However, the estimated roughness when using realized volatility is much rougher than the true roughness, and realized variance appear even rougher in this example compared to the previous one. As this is a simulation study this rougher behaviour of realized volatility purely comes from the estimation error, and this illustrates how estimation errors can substantially distort the roughness estimate.

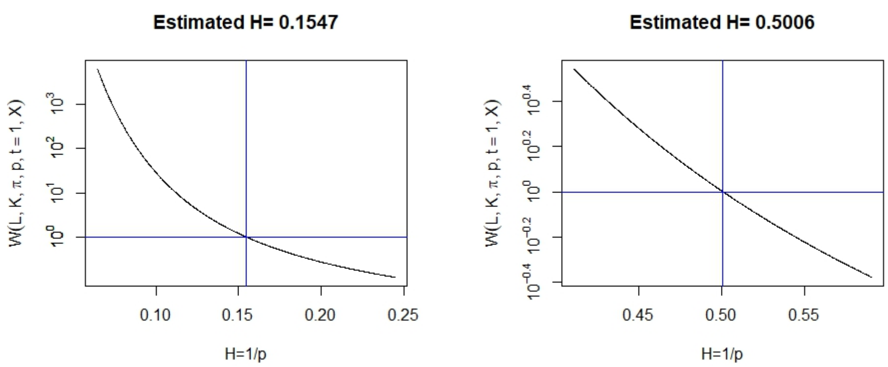


Figure 16: The value of $\log(W(L = 300 \times 300, K = 300, \pi, p, t = 1, X))$ plotted against $H = 1/p$ in black. The blue vertical line represents the estimated roughness $\hat{H}_{L,K}$. **Left:** Estimated roughness index $\hat{H}_{L,K}$ for realized volatility derived from the stochastic volatility model (17). **Right:** Estimated roughness index for instantaneous volatility of the same price path.

Now we use the roughness estimator by logarithmic regression $\hat{H}_R$ for the same instantaneous volatility and realized volatility data. In Figure 17 we display the results for the roughness estimator when using instantaneous volatility. The estimated roughness index is $\hat{H}_R = 0.498$ which is very close to the true roughness of the model $H = \frac{1}{2}$. This indicates that the roughness estimator performs well for instantaneous volatility. In Figure 18 we display the corresponding results for the log regression estimator $\hat{H}_R$ when using realized volatility as input. Here we obtain an estimated roughness of $\hat{H}_R = 0.089$ which is even rougher than the estimate we obtained for the estimator $\hat{H}_{L,K}$ via $p$-th variation. This rougher behaviour purely comes from the estimation error, and this once again illustrates that using realized volatility for roughness estimation can lead to a dramatic underestimation of the true roughness of the underlying model.

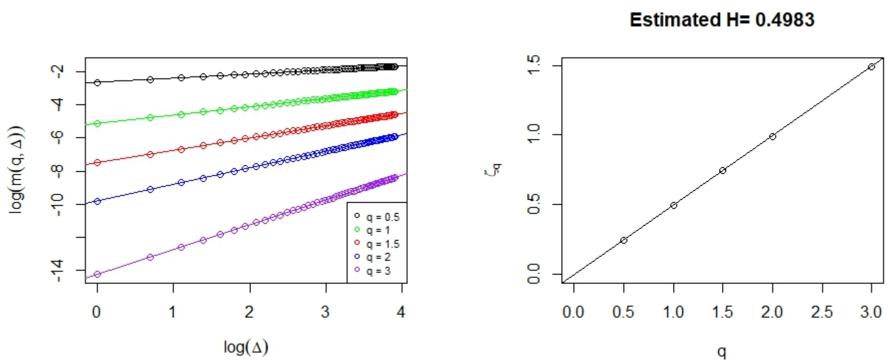


Figure 17: Roughness estimation by log regression using instantaneous volatility simulated from model (19). **Left:** $\log(m(q,\Delta))$ plotted against $\log(\Delta)$. **Right:** Regression coefficients $\zeta_q$ plotted against $q$. The estimated roughness index is $\hat{H}_R = 0.498$.

We will now use the sequential scale estimator for the same price path. We will be using $n = 11$ and $m_n = 2^{11}$ for the estimation. Furthermore, we use the parameters $m = 4$ and $\alpha_k = 1$ for $k = 0, 1, 2, 3$ for the computation of $\widehat{\mathscr{R}}^s_n$. As in Section 4.1 we will rescale the price process such that our observed data points fit the required input for the sequential scale estimator. To this end, we need $2^{n+13}$ data points on the time interval $[0, 1]$. We set $\Delta t = 2^{-n-13}$ and rescale our $\Delta B_t$ and $\Delta B'_t$ to this new $\Delta t$. We then compute $S_t$ as in (19) using these rescaled $\Delta t$, $\Delta B_t$ and $\Delta B'_t$. We compute realized variance $\hat{Y}^{(n)}_t$ as in (13) and $Y_t(\sigma)$ as in (18).
In Figure 19 we have plotted these two approximations of integrated variance $y(t)$ and their difference. The left plot of Figure 13 represent the realized variance in black and the approximation $Y(\sigma_t)$ as in (18) in red. The middle plot shows the difference between these two approximations of integrated variance, and the right plot shows the difference between the log of the two approximations. Just as in the previous example we observe that the difference between

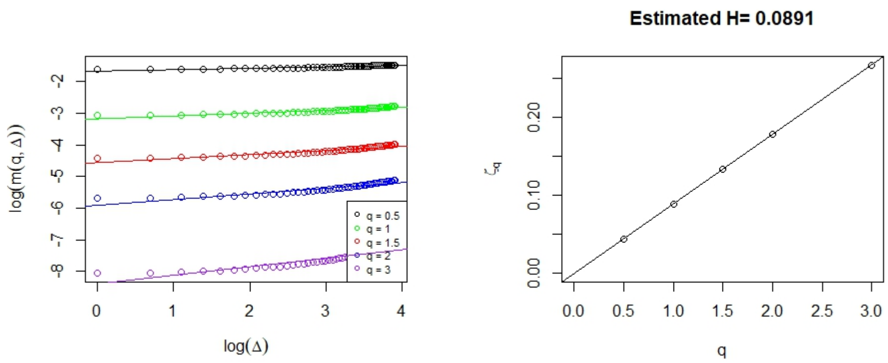


Figure 18: Roughness estimation by log regression using realized volatility for a price path simulated from model (19). **Left:** $\log(m(q, \Delta))$ plotted against $\log(\Delta)$. **Right:** Regression coefficients $\zeta_q$ plotted against $q$. The estimated roughness index is $\hat{H}_R = 0.089$.

realized variance and integrated variance is very small. The two lines in the left plot cannot be distinguished, and the difference is even smaller in this example. However, the log difference is still much bigger for the very first points compared to the remaining points.

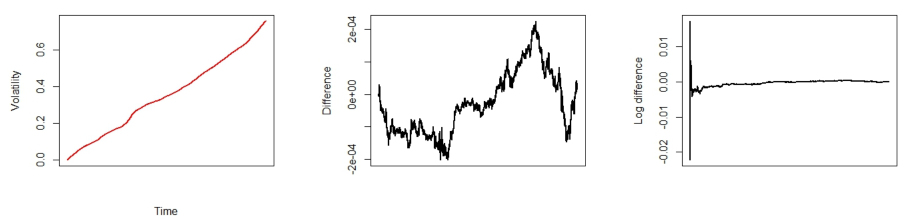


Figure 19: Integrated variance of the original path from model (19) rescaled to fit the sequential scale estimator. **Left:** The red line represents $Y$ computed directly from instantaneous volatility $\sigma_t$ whereas the black line represents realized variance $\hat{Y}_t^{(n)}$. **Middle:** Corresponding difference between the lines in the left plot. **Right:** Corresponding log difference.

In Table 4 we display the results from the sequential scale roughness estimation. We observe that the sequential scale estimate when using integrated variance $Y_t(\sigma)$ as input $\widehat{\mathscr{R}}_n^s(Y) = 0.433$ is not very accurate but still somewhat close to the true roughness of the model $H = \frac{1}{2}$ . However, when using realized variance as input we obtain the roughness estimate $\widetilde{\mathscr{R}}_n^s(S) = 0.130$ for the sequential scale estimator which is much rougher than the true roughness of the model and quite close to the roughness estimates obtained for realized volatility by the two other estimators. Thus, the very small difference between $\hat{Y}_t^{(n)}$ and $Y(\sigma_t)$ observed in Figure 19 completely changes the estimates. Furthermore, we see that while $\widehat{\mathscr{R}}_n^s$ improves the original scale estimate when using integrated variance, it is less accurate than the original scale estimator $\widetilde{\mathscr{R}}_n$ when estimating roughness from realized variance. However, both versions of the estimator performs poorly when input is realized variance, and when using $n = 11$ we would expect some variation in the estimates, so clear conclusions should not be drawn from just a single path.

| | Realized variance | Integrated variance $Y_t(\sigma)$ |
|---|---|---|
| Sequential scale estimator | $\widetilde{\mathscr{R}}_n^s(S) = 0.1298$ | $\widehat{\mathscr{R}}_n^s(Y) = 0.4328$ |
| Original scale estimator | $\widetilde{\mathscr{R}}_n(S) = 0.2924$ | $\widehat{\mathscr{R}}_n(Y) = 0.4177$ |

Table 4: The roughness estimates from the sequential scale roughness estimator with $n = 11$ and $m_{11} = 2^{11}$ for model (19) by using respectively realized variance and the approximation of integrated variance from instantaneous volatility $Y_t(\sigma)$.

We now compute the distributions of the estimated roughness index via normalized $p$-th statistic $\widehat{H}_{L,K}$ with $L = 300 \times 300$ and $K = 300$ for realized volatility and instantaneous volatility. We generate the distributions across 2500 independent paths drawn from the OU-SV model (19). The left plot of Figure 21 is the distribution of $\widehat{H}_{L,K}$ for realized volatility whereas the right plot is the corresponding distribution for instantaneous volatility as input to the roughness estimator. In addition to this, Table 5 provides the summary statistics for the roughness estimator $\widehat{H}_{L,K}$ for realized and instantaneous volatility respectively across the 2500 independent paths. We observe that realized volatility systematically exhibit much rougher behaviour than instantaneous volatility. The roughness estimates based on instantaneous volatility are very close to the roughness of the true model $H = 0.5$. However, the roughness estimates generated from realized volatility are much smaller with a mean of $\widehat{H}_{L,K} = 0.1549$ across the 2500 independent simulations. The variations of the volatility estimates are very similar for the two density plots. Both distribution plots only show a small variation indicating that the estimates are quite stable.

Note that our results deviates slightly from the results in Cont and Das [2024] for a similar model. This might be caused by Cont and Das [2024] using the mean of $\sigma_t$ across the 300 consecutive data points as their instantaneous volatility which creates a slightly smoother volatility process. Furthermore, Cont and Das [2024] might be using a different $T$ than us which in the OU-SV model will impact the size of the estimation error and thus the estimated roughness index

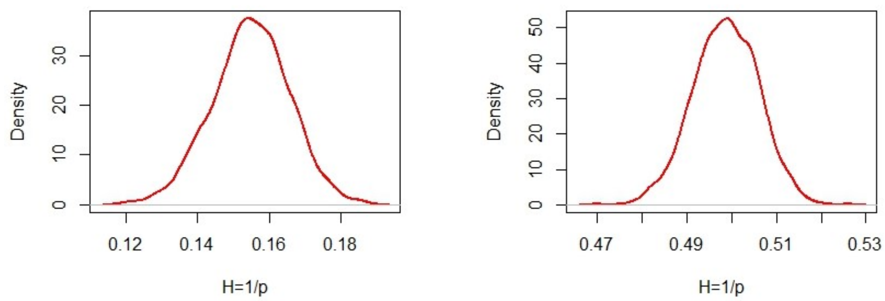


Figure 20: Distribution of the estimated roughness index $\widehat{H}_{L,K}$ via normalized $p$-th variation using $L = 300\times300$ and $K = 300$ across 2500 independent simulations of the OU-SV model (19). **Left:** Realized volatility. **Right:** Instantaneous volatility.

| | Realized volatility | Instantaneous volatility |
|---|---|---|
| Min. | 0.1192 | 0.4698 |
| 1st quartile | 0.1480 | 0.4938 |
| Median | 0.1551 | 0.4988 |
| Mean | 0.1549 | 0.4987 |
| 3rd quartile | 0.1621 | 0.5039 |
| Max. | 0.1873 | 0.5257 |

Table 5: Summary of statistics for estimated roughness index $\hat{H}_{L,K}$ for realized and instantaneous volatility across 2500 independent simulations the OU-SV model (19) with $L = 300 \times 300$ and $K = 300$.

for realized volatility when all other parameters are kept constant. The conclusions are however the same. Realized volatility does systematically exhibit much rougher behaviour than instantaneous volatility and than the true roughness of the model. This rougher behaviour is solely caused by the estimation error, and it indicates that roughness estimated based on realized volatility can be unreliable.

In Figure 21 we have made density plots for the other roughness estimators across 150 independent paths generated from the OU-SV model (19). The left plot of Figure 21 displays density plots of the estimators when used on realized volatility and realized variance whereas the right plot displays density plots when using instantaneous volatility and integrated variance $Y(\sigma_t)$ as input to the estimators. The density plot of the roughness estimator by log regression $\widehat{H}_R$ is represented by the red line. It has very little variation in its estimates. For instantaneous volatility it accurately estimates the true roughness of the underlying model whereas it for realized volatility systematically provides a roughness estimate near 0.09 which is much rougher than the true roughness exponent $H = \frac{1}{2}$ and also rougher than the estimates from the roughness index estimator via $p$-th variation.
For the sequential scale estimator, we observe that it for integrated variance seems to be an unbiased estimator of the true roughness of the underlying model. However, $\widehat{\mathscr{R}}_n^s$ does have significantly more variation than the roughness estimator via log regression $\widehat{H}_R$. When using realized variance as input, the sequential scale estimator $\widetilde{\mathscr{R}}_n^s$ does not estimate the true roughness of spot volatility well. It systematically underestimates the true roughness. However, it does seem to slightly improve the roughness estimate via log regression $\widehat{H}_R$, and $\widetilde{\mathscr{R}}_n^s(S)$ has a mean near 0.2. Also in this case the sequential scale estimator has some variation which is expected when $n$ is chosen to be $n = 11$. However, $m_n = 11$ is chosen to be quite large to avoid distortion from proxy errors, but the proxy errors in realized variance does lead to a systematic underestimation of the true roughness of the model.

For this example, the sequential scale estimator $\widetilde{\mathscr{R}}_n^s$ is an improvement of the original scale estimator $\widetilde{\mathscr{R}}_n$. We observe from Figure 21 that the original scale estimator $\widetilde{\mathscr{R}}_n$ has a very big variation and generates completely unreliable results both for integrated variance and realized variance. This corresponds to our findings in the simulation examples in Section 3.4.2. There we found that when the volatility process is a scaling of an underlying model then the original scale estimator $\widetilde{\mathscr{R}}_n$ performs very poorly. In this OU-SV model (19) the volatility process is the log of another underlying process, and that distorts the outcome of the original scale estimation.

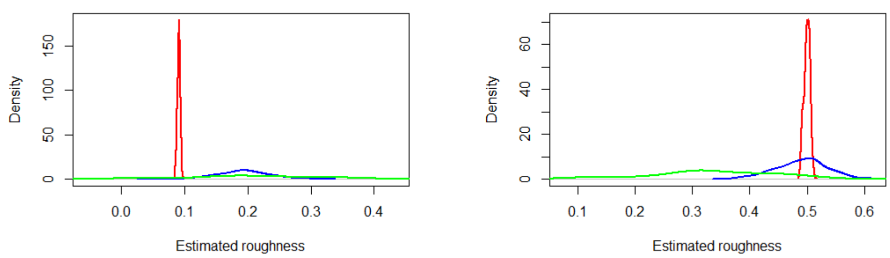


Figure 21: Density plots of the roughness estimators $\widehat{H}_R$ (red), $\widetilde{\mathscr{R}}^s_n(S)$ and $\widehat{\mathscr{R}}^s_n(Y)$ (blue), and $\widetilde{\mathscr{R}}_n(S)$ and $\widehat{\mathscr{R}}_n(Y)$ (green) across 150 independent paths drawn from the OU-SV model (19). **Left:** Using realized volatility and realized variance as input. **Right:** Using instantaneous volatility $\sigma_t$ and integrated variance $Y(\sigma_t)$ as input.

### 4.3 A fractional Ornstein-Uhlenbeck model

In the two previous models, instantaneous volatility follows a diffusive behaviour similar to a Brownian motion with $H = 0.5$. We now consider a more general case of a stochastic volatility model where the volatility process has a general roughness index $H \in (0, 1)$ generated from a fractional Brownian motion. We investigate the model for different roughness indices and explore how this affect the estimation error and estimated roughness. Consider the following process where the volatility is described by a fractional Ornstein-Uhlenbeck model:

$$dS_t = S_t \sigma_t dB_t, \quad \sigma_t = \sigma_0 e^{Z_t}, \quad dZ_t = -\gamma Z_t\, dt + \theta\, dB^H_t, \tag{20}$$

where $S_t$ is the price process, $B_t$ is a Brownian motion, and $B^H_t$ is a fractional Brownian motions with Hurst exponent $H$. For the simulations we use the parameters $\sigma_0 = \gamma = \theta = 1$ and $Z_0 = 0$, and we set $T = 5$ and $S_0 = 1$.

We now repeat the procedure described in Section 4.1 to compute the estimated roughness index $\widehat{H}_{L,K}$ with $L = 300 \times 300$ and $K = 300$ for realized and instantaneous volatility. Furthermore, we compute the roughness estimator via logarithmic regression for the same realized and instantaneous volatility data. We compute these roughness estimates across different values of Hurst parameters $H$ for the underlying model.
In Table 6 we have computed roughness estimates for volatility data from the fractional Ornstein-Uhlenbeck model (20) with Hurst exponent $H = \{0.1, 0.2, 0.3, 0.4, 0.5, 0.6, 0.7, 0.8\}$. We have used the same seed in the simulation for all values of $H$ such that the underlying stochastic element of the price processes is the same. Thus, the difference between the price processes solely lies in the Hurst exponent $H$.

The corresponding paths for the price process, realized volatility and instanta-

| H | IV ($p$-th) | RV ($p$-th) | IV (log reg) | RV (log reg) |
|---|---|---|---|---|
| 0.1 | 0.126 | 0.199 | 0.102 | 0.197 |
| 0.2 | 0.220 | 0.256 | 0.204 | 0.250 |
| 0.3 | 0.313 | 0.261 | 0.305 | 0.257 |
| 0.4 | 0.408 | 0.218 | 0.407 | 0.188 |
| 0.5 | 0.504 | 0.159 | 0.508 | 0.095 |
| 0.6 | 0.598 | 0.102 | 0.607 | 0.036 |
| 0.7 | 0.691 | 0.070 | 0.703 | 0.012 |
| 0.8 | 0.778 | 0.052 | 0.794 | 0.004 |

Table 6: Estimated roughness via $p$-th variation $\widehat{H}_{L,K}$ and via log regression for instantaneous and realized volatility for simulated data from a fractional Ornstein-Uhlenbeck model (20) with Hurst exponent $H = \{0.1, 0.2, 0.3, 0.4, 0.5, 0.6, 0.7, 0.8\}$.

neous volatility from model (20) with Hurst exponent $H = \{0.1, 0.2, 0.3, 0.4, 0.5, 0.6, 0.7, 0.8\}$ are presented in Figure 22. Visually we observe that the price processes do not differ much as the Hurst exponent changes. However, the paths of realized and instantaneous volatility are very different for different Hurst exponents. For small Hurst exponents instantaneous volatility does visually appear more rough than realized volatility. However, instantaneous volatility becomes smoother and smoother as $H$ increases. That is expected since increasing the Hurst exponent $H$ implies that the volatility process becomes smoother. However, realized volatility is not gradually getting smoother as $H$ increases. Instead we observe that for large Hurst exponents, realized volatility appears very rough. This is supported by the roughness estimates in Table 6. The estimated roughness based on instantaneous volatility is increasing as $H$ increases both for the roughness estimator via $p$-th variation and the roughness estimator via logarithmic regression. The estimated roughness based on realized volatility is increasing at first as $H$ increases, but for large Hurst exponents the estimated roughness decreases and the estimated roughness of the realized volatility process is estimated to be very rough when the true Hurst exponent is $H = 0.8$.

As Figure 22 visually indicates, the realized volatility paths do seem to be rougher than corresponding spot volatility paths when we obtain roughness estimates for realized volatility that are much lower than the true roughness of the underlying model. We have no reason to believe that the roughness estimators are inaccurate if given the correct input since they work as a good estimate for instantaneous volatility data. It is likely that the realized volatility paths are more alike paths generated from a model with a rougher roughness exponent, and the estimates obtained are as such not surprising. However, when the estimates for realized volatility are meant to be a roughness estimate of the underlying model, the estimates turn out to be poor. This two-step approach of first estimating proxy values of volatility $\hat{\sigma}_t$ (i.e. realized volatility) and then

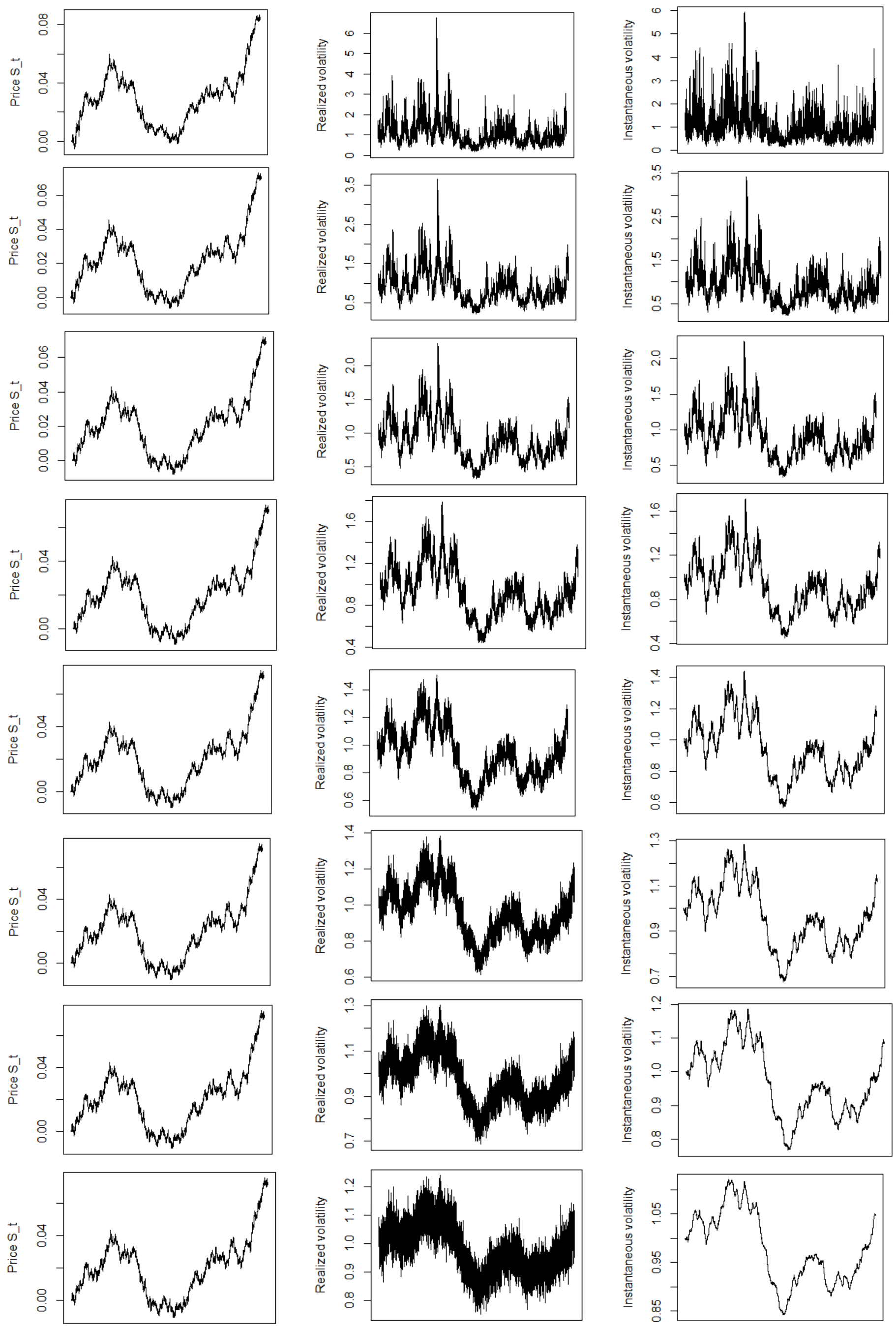

Figure 22: **Left:** Simulated price path $S_t - S_0$ of fractional OU model 20 with Hurst exponent $H = \{0.1, 0.2, 0.3, 0.4, 0.5, 0.6, 0.7, 0.8\}$ respectively. **Center:** Realized volatility. **Right:** Instantaneous volatility.

using these proxy values as input to estimators that we know works for spot volatility data $\sigma_t$ therefore turns out to be very problematic.

In Figure 23 we have plotted the values from Table 6 in a graph. The blue lines represents roughness estimates for instantaneous volatility while the red lines represents roughness estimates for the corresponding realized volatility. The solid lines are the estimated roughness index via $p$-th variation $\widehat{H}_{L,K}$ with $L = 300 \times 300$ and $K = 300$ while the dashed lines represent roughness estimates via logarithmic regression. The $x$-axis represents the true value of $H$ of the simulated fractional OU model. We observe that roughness estimates based on instantaneous volatility give accurate estimates of the true Hurst index $H$. However, the estimated roughness for realized volatility turns out to be a poor estimate of the true roughness of the underlying model, and it always stay below 0.3. In particular, when the instantaneous volatility process is generated from a smooth process (i.e. $H > \frac{1}{2}$) the roughness estimate of realized volatility is very far from the true roughness of the model.
It seems that our two roughness estimates coincides and generate similar estimates. Only when the true model is smooth (i.e. $H > 0.5$) the roughness estimate by logarithmic regression for realized volatility seems to systematically be rougher that the corresponding roughness estimate via $p$-th variation. However, both estimates are very far from the true roughness of the underlying model in this case.

In Figure 24 we have repeated the above analyses for 100 independent simulated prices processes generated by the fractional Ornstein-Uhlenbeck model (20) but only for the estimated roughness index via $p$-th variation $\widehat{H}_{L,K}$ with $L = 100 \times 100$ and $K = 100$. The figure shows the estimators $\widehat{H}_{L,K}(RV)$ and $\widehat{H}_{L,K}(\sigma)$ plotted against Hurst exponents $H = \{0.1, 0.2, 0.3, 0.4, 0.5, 0.6, 0.7, 0.8\}$ for every independent path. The bold black lines represent the mean across 100 independent simulations whereas the dotted lines represent the corresponding 75% confidence interval. If equation (9) have no solution for $H \in (0, 1)$ we set $\widehat{H}_{L,K} = 0$.

From Figure 24 we observe that for all 100 independent simulations, the roughness estimators exhibit a similar behaviour. Our conclusions about the poorness of roughness estimates for realized volatility still hold and was not just a matter of the single price path we studied before. In particular, for the fractional Ornstein-Uhlenbeck model (20) realized volatility always exhibit rough behaviour (i.e. $H < \frac{1}{2}$) no matter what the true roughness of the underlying volatility process is. The estimated roughness based on instantaneous volatility is quite accurate and as this is a simulation study we have no measurement errors so the inaccuracy of the estimators for realized volatility solely comes from the estimation error.

We now introduce the sequential scale estimator $\widehat{\mathscr{R}}_n^s$ to this example. We take a

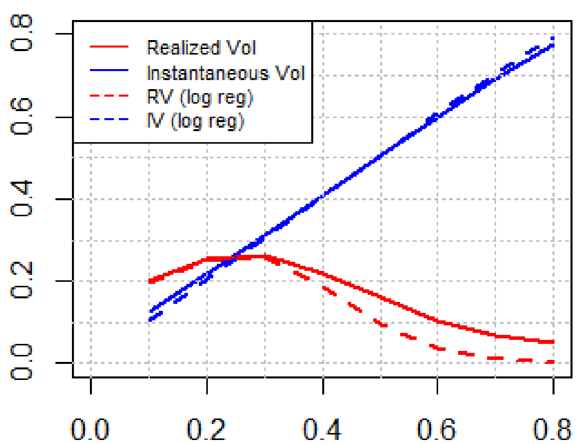


Figure 23: Estimated roughness indexes for realized and instantaneous volatility from a fractional OU model (20) plotted for price paths generated by different values of $H$. The solid lines are roughness indexes via $p$-th variation $\widehat{H}_{L,K}$ with $L = 300 \times 300$ and $K = 300$ while the dashed lines represents estimated roughness by logarithmic regression.

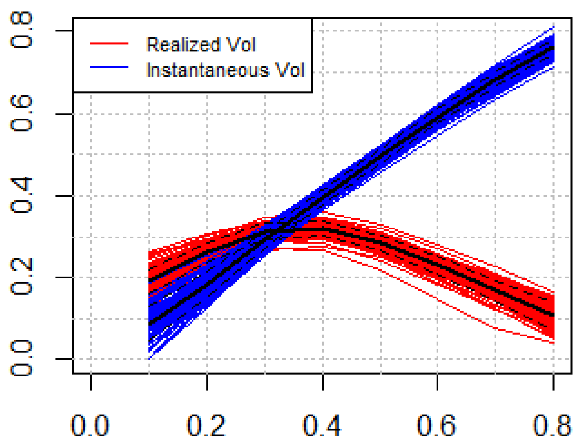


Figure 24: Estimated roughness index via $p$-th variation for realized and instantaneous volatility plotted against different values of $H$ for 100 independent price paths from a fractional OU model (20). The solid black lines represent the mean across the 100 paths and the dashed black lines represent the corresponding 75% confidence interval.

slightly different approach than in the previous examples and simulate directly the required observations needed for the sequential scale estimator from model (20) with $T = 1$. Once again we need to decide the trade-off between using our generated points in each realized variance calculation or simply to make more realized variance calculations which generates more input to the estimator. That is, if we increase $m_n$ we use more data points for each realized variance interval making the realized variance calculations more accurate which is useful to avoid distortion from proxy errors. Meanwhile, by increasing $n$ we generate more realized variance intervals and observations of cumulative realized variance such that the estimator gets more data input making it more consistent in its estimates.
By the condition in Theorem 1 we need $\lim_{n\uparrow\infty} \frac{1}{n}\log_2 m_n > 2H$ to be sure that $\widehat{\mathscr{R}}_n$ and $\widetilde{\mathscr{R}}_n$ converge to the same limit. We will use $n = 10$ and $m_{10} = 2^{12}$ for the estimation. Thus, we have $\frac{1}{n}\log_2 m_n = 1.2$ for $n = 10$. For $H > 0.6$ we then do not have $\frac{1}{n}\log_2 m_n > 2H$ and we could therefore expect distortion from proxy errors for $H = \{0.7, 0.8\}$. However, there is a trade-off between using a large $n$ and a large $m_n$, and to avoid making the data to computationally challenging to compute we find that $n = 10$ and $m_{10} = 12$ is the best way to demonstrate the performance of the sequential scale estimator for this example.

For the same price path we also compute the roughness index via $p$-th variation $\widehat{H}_{L,K}$ and the roughness estimator via log regression $\widehat{H}_R$ by computing instantaneous and realized volatility for every 300 consecutive points. Thus, we use $L =?$ and $K = \sqrt{L}$ for the estimator $\hat{H}_{L,K}$. In Table 7 we display the roughness estimates obtained for Hurts exponent $H = \{0.1, .0.2, 0.3, 0.4, 0.5, 0.6, 0.7, 0.8\}$. We have used the same seed for all $H$ values. The estimates from $\widehat{\mathscr{R}}^s_n$ are displayed in the two columns furthest to the right in Table 7. IV should for this estimator be understood as integrated variance approximated directly from instantaneous volatility as in (18) whereas RV should be understood as realized variance computed as in (13). For $\widehat{H}_{L,K}$ and $\widehat{H}_R$ we obtain similar results to the estimates from Table 6 and both of these estimates are inaccurate when used for realized volatility and always stay below 0.3. However, the absolute scale estimator $|\widehat{\mathscr{R}}^s_n|$ performs differently. We observe that the estimator is accurate when using spot variance $Y(\sigma_t)$ as input. When using realized variance as input the estimator is not very accurate, but it performs better than the other two roughness estimators, and it does not estimate the process to be rough (i.e. $H < \frac{1}{2}$) when the true underlying model is actually smooth (i.e. $H > \frac{1}{2}$).

In the left plot of Figure 25 we have plotted the results from Table 7 to visualize the estimates. The right plot of Figure 25 shows roughness estimates from the absolute scale estimator $|\widehat{\mathscr{R}}^s_n|$ across 100 independent price paths plotted against the true roughness of the model $H = \{0.1, 0.2, 0.3, 0.4, 0.5, 0.6, 0.7, 0.8\}$. Thus, it is 100 repetitions of the procedure described above. The bold black lines represent the mean acroos 100 independent simulations whereas the dotted lines represent a 75% confidence interval.

| H | IV ($\widehat{H}_{L,K}$) | RV ($\widehat{H}_{L,K}$) | IV ($\widehat{H}_R$) | RV ($\widehat{H}_R$) | IV ($|\widehat{\mathscr{R}}_n^s|$) | RV ($|\widehat{\mathscr{R}}_n^s|$) |
|---|---|---|---|---|---|---|
| 0.1 | 0.140 | 0.226 | 0.102 | 0.192 | 0.067 | 0.175 |
| 0.2 | 0.219 | 0.275 | 0.202 | 0.246 | 0.189 | 0.294 |
| 0.3 | 0.312 | 0.275 | 0.300 | 0.259 | 0.294 | 0.445 |
| 0.4 | 0.408 | 0.216 | 0.399 | 0.201 | 0.396 | 0.501 |
| 0.5 | 0.503 | 0.150 | 0.498 | 0.109 | 0.498 | 0.510 |
| 0.6 | 0.593 | 0.107 | 0.596 | 0.044 | 0.599 | 0.510 |
| 0.7 | 0.676 | 0.077 | 0.691 | 0.016 | 0.699 | 0.509 |
| 0.8 | 0.749 | 0.055 | 0.780 | 0.005 | 0.799 | 0.508 |

Table 7: Estimated roughness for the three roughness estimators $\widehat{H}_{L,K}$, $\widehat{H}_R$ and $|\widehat{\mathscr{R}}_n^s|$ using instantaneous volatility (IV) and realized volatility/variance (RV) for simulated data from a fractional Ornstein-Uhlenbeck model (20) with Hurst exponent $H = \{0.1, 0.2, 0.3, 0.4, 0.5, 0.6, 0.7, 0.8\}$.

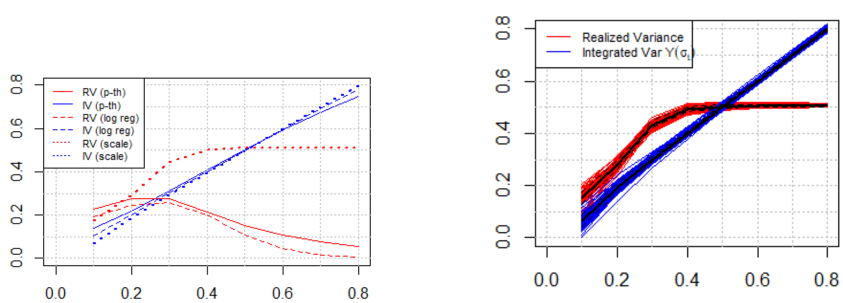


Figure 25: Estimated roughness indexes using instantaneous volatility (IV) and realized volatility/variance (RV) from a fractional OU model (20) with $T = 1$ plotted for price paths generated by different values of $H$. **Left:** Estimates for all three roughness estimators $\widehat{H}_{L,K}$, $\widehat{H}_R$ and $|\widehat{\mathscr{R}}_n^s|$ . **Right:** Absolute scale estimates $|\widehat{\mathscr{R}}_n^s|$ for 100 independent price paths. The solid black line represents the mean, and the dashed black lines represent a 75% confidence interval.

From Figure 25 we conclude that the scale estimator systematically exhibits the same kind of behaviour. That is, when used for realized variance the estimator is not very precise especially when the true roughness exponent of the underlying model takes a high value. However, it does remedy some of the inaccuracies observed for the other two estimators, and it does not estimate the path to be rough when the underlying model is not rough. As this is a simulation study, the difference between the blue and red lines are solely caused by estimation errors.

In practice, instantaneous volatility cannot be observed, and roughness estimates are based on realized volatility. If using traditional roughness estimators such as $\widehat{H}_{L,K}$ and $\widehat{H}_R$, the above examples illustrate that one cannot necessarily draw the conclusion that (spot) volatility is rough just because realized volatility exhibit rough behaviour with $\hat{H}_{L,K}(RV) < \frac{1}{2}$ even if the estimated roughness is well below $\frac{1}{2}$.
Passing to the absolute sequential scale estimator $|\widehat{\mathscr{R}}^s_n|$ which is developed with the ambition of accurately estimating roughness from realized variance does in these examples improve estimation from realized input. However, $|\widehat{\mathscr{R}}^s_n|$ is also somewhat vulnerable to estimation errors and does not completely remove inaccuracies caused by estimation errors. Furthermore, $|\widehat{\mathscr{R}}^s_n|$ requires observations of realized variance for very specific time points making it less applicable to real time high frequency data.

## 4.4 RFSV model

We will now consider the Rough Fractional Stochastic Volatility (RFSV) model suggested by Gatheral et al. [2018]. The model is defined in the following way:

$$dS_t = S_t \sigma_t dB_t, \quad \sigma_t = e^{Z_t}, \quad dZ_t = -\alpha(Z_t - z_0)\, dt + \nu\, dB_t^H, \tag{21}$$

for some $\nu > 0$, $\alpha > 0$, $z_0 \in \mathbb{R}$ and $H < \frac{1}{2}$ where $B_t$ is a Brownian motion and $B_t^H$ is a fractional Brownian motion. Gatheral et al. [2018] further argues that choosing $\alpha \ll \frac{1}{T}$ is desirable since the log-volatility then locally behaves like a fBm while it is still technically stationary. In addition to this, Gatheral et al. [2018] argues that observed skew term structure in financial data can easier be replicated by choosing $\alpha \ll \frac{1}{T}$.

The specified RFSV model is similar to model (20) from Section 4.3 and both models use a fractional Ornstein-Uhlenbeck process to model log-volatility. When simulating from the model we use the parameters $\nu = 0.3$, $\alpha = 5 \cdot 10^{-4}$, $z_0 = -5$ and we set $Z_0 = z_0$, $S_0 = 1$ and $T = 5$. These parameter values are the values that Gatheral et al. [2018] suggest for the RFSV model chosen to be consistent with their empirical findings. Furthermore, Gatheral et al. [2018] suggest $H = 0.14$ to be consistent with realized volatility signals. However, we will be simulating from the model using different Hurst parameter values in order to properly investigate the behaviour of the roughness estimators. We will also not restrict ourselves to $H < \frac{1}{2}$ even though it is specified like that for the RFSV model. For $H > \frac{1}{2}$ the model actually becomes the original FSV model introduced by Comte and Renault [1998]. Since we only want to investigate if roughness estimates for this model are reliable it makes since to combine RFSV and FSV into one model in this example such that we can use the model with $H \in (0, 1)$.

We use the same procedure as in the previous examples and calculate realized variance across 300 consecutive points. We will be using $L = 150 \times 150$ and $K = 150$ for this example. For the sequential scale estimator we will use $n = 9$ and $m_9 = 11$, and for this estimator we will rescale the price process to the required number of points on the time interval $t \in [0, 1]$. In Table 8 we display the obtained roughness estimates from the RSFV model (21) with Hurst exponent $H = \{0.1, 0.2, 0.3, 0.4, 0.5, 0.6, 0.7, 0.8\}$. Furthermore, on the left plot of Figure 26 we have plotted the roughness estimates from Table 8 against the true Hurst parameter of the underlying model to visualize the results. The right plot of Figure 26 display estimates from the roughness estimator via log regression $\widehat{H}_R$ for 100 independent price paths simulated for all Hurst parameters $H = \{0.1, 0.2, 0.3, 0.4, 0.5, 0.6, 0.7, 0.8\}$.

| H | IV ($\widehat{H}_{L,K}$) | RV ($\widehat{H}_{L,K}$) | IV ($\widehat{H}_R$) | RV ($\widehat{H}_R$) | IV ($\widehat{\mathscr{R}}^s_n$) | RV ($\widetilde{\mathscr{R}}^s_n$) |
|---|---|---|---|---|---|---|
| 0.1 | 0.104 | 0.148 | 0.106 | 0.165 | 0.023 | 0.018 |
| 0.2 | 0.194 | 0.149 | 0.210 | 0.175 | 0.134 | 0.111 |
| 0.3 | 0.293 | 0.123 | 0.311 | 0.140 | 0.251 | 0.166 |
| 0.4 | 0.396 | 0.103 | 0.412 | 0.085 | 0.366 | 0.146 |
| 0.5 | 0.498 | 0.084 | 0.511 | 0.043 | 0.477 | 0.054 |
| 0.6 | 0.599 | 0.065 | 0.611 | 0.019 | 0.585 | -0.088 |
| 0.7 | 0.698 | 0.046 | 0.711 | 0.008 | 0.692 | -0.256 |
| 0.8 | 0.790 | 0.028 | 0.807 | 0.004 | 0.797 | -0.418 |

Table 8: Estimated roughness for the three roughness estimators $\widehat{H}_{L,K}$, $\widehat{H}_R$ and $\widehat{\mathscr{R}}^s_n$ using instantaneous volatility (IV) and realized volatility/variance (RV) for simulated data from a RFSV model (21) with Hurst exponent $H = \{0.1, 0.2, 0.3, 0.4, 0.5, 0.6, 0.7, 0.8\}$.

We observe from the table and figure that the roughness estimates behave in a similar way to what we saw for the fOU model in Section 4.3. That is, realized volatility always exhibit rough behaviour, and roughness estimates for realized volatility data turn out to be a very poor estimate for the true roughness of the underlying model especially when the underlying model is diffusive or smooth (i.e. $H \geq \frac{1}{2}$). We observe that realized volatility actually exhibit even more rough behaviour in this example compared to the fOU model. The estimates for realized volatility always stay below 0.2 meaning that the estimation error

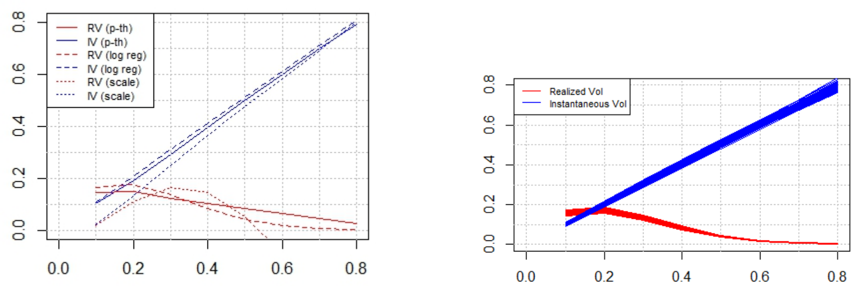


Figure 26: Roughness estimates using instantaneous volatility (IV) and realized volatility/variance (RV) from a RFSV model (21) plotted for price paths generated by different values of $H$. **Left:** Estimates for all three roughness estimators $\widehat{H}_{L,K}$, $\widehat{H}_R$ and $\widehat{\mathscr{R}}^s_n$ . **Right:** Roughness estimates via log regression $\widehat{H}_R$ for 100 independent price paths.

distorts the roughness estimation even more for the RFSV model. However, the roughness estimates for instantaneous volatility seems to be even more accurate for this example compared to the previous one.
The sequential scale estimator for realized variance $\widetilde{\mathscr{R}}^s_n$ estimates the true roughness of the underlying model very poorly. For $H = \{0.6, 0.7, 0.8\}$ it provides negative roughness estimates which are values that roughness can never have. However, as we saw in Figure 25 in the previous example, the variation of $\widetilde{\mathscr{R}}^s_n$ is quite big, and it is difficult to conclude anything from just a single path. But Figure 26 indicates that the sequential scale estimator is only somewhat accurate for realized variance for $H = \{0.1, 0.2, 0.3\}$. In general, the RFSV model seems to be even more vulnerable to distortion from estimation errors than what we saw in the previous examples.

Gatheral et al. [2018] also make a simulation example for the RFSV model (21). They use the same parameter values as we have used, and they set $H = 0.14$. From this simulation they estimate the roughness based on realized volatility and obtain an estimate close to the true roughness of the model $H = 0.14$ which they use as a verification of the model and the roughness estimator. However, Figure 26 illustrates that only for Hurst parameters $H$ in the range $H \approx 0.15$ do instantaneous volatility and realized volatility exhibit the same kind of roughness behaviour for the RFSV model. It seems to be a coincidence that Gatheral et al. [2018] use a Hurst parameter where they do not observe the distortion estimation error can cause when estimating roughness from realized volatility.
Overall, this example once again illustrate that realized volatility tends to always exhibit rough behaviour, and one cannot necessarily conclude that the

underlying spot volatility process is rough just because estimated roughness of realized volatility is rough.

# 5 Conclusion

In this thesis we have investigated roughness of volatility processes in financial time series and taken a closer look at the claim 'volatility is rough'. More precisely, we have investigated the robustness of roughness estimates based on realized volatility for three different roughness estimators. Most roughness estimators in literature rely on approximating true spot volatility $\sigma_t$ by realized volatility and then estimating the roughness of these proxy values $\hat{\sigma}_t$. We introduce two roughness estimators based on this approach, the roughness estimator via normalized $p$-th variation statistics $\widehat{H}_{L,K}$ and the roughness estimator by logarithmic regression $\widehat{H}_R$. We have in this thesis shown that such estimates based on realized volatility can be unreliable. We have conducted numerical experiments, and as described in section 4.1 and 4.2 we find that for two stochastic volatility diffusion models driven by a Brownian motion, realized volatility exhibit rough behaviour with an estimated roughness index significantly smaller than the true roughness index $H = \frac{1}{2}$. For our two stochastic diffusive examples we estimate the roughness of realized volatility in the range $\widehat{H} \approx 0.3$ and $\widehat{H} \approx 0.15$ respectively. However, when estimating directly from instantaneous volatility we obtain accurate results very close to the true roughness of the underlying model $H = \frac{1}{2}$. The two estimators $\widehat{H}_{L,K}$ and $\widehat{H}_R$ widely coincides, and generate very similar results in all cases. As these are simulation examples, this apparent rough behaviour of realized volatility is entirely caused by the difference between realized volatility and instantaneous volatility also known as the estimation error. These results suggest that it cannot necessarily be concluded that observed rough behaviour in realized volatility is an indicator of similar behaviour in true spot volatility.

Moreover, we show in section 4.3 and 4.4 that for volatility processes driven by a fractional Ornstein-Uhlenbeck model, realized volatility always exhibit rough behaviour (i.e. $\widehat{H} < \frac{1}{2}$). For both of these examples even when the true underlying model has diffusive or smooth behaviour (i.e. $H \geq \frac{1}{2}$) the roughness estimates based on realized volatility always stay below 0.3. If we estimate roughness directly from instantaneous volatility we obtain accurate estimates, and this again indicates that the estimation error can substantially distort the outcome of the roughness estimation. More precisely, these results show that stochastic diffusive models or even smooth volatility processes are perfectly compatible with rough behaviour observed in realized volatility. The conclusions from 'rough volatility' literature such as Gatheral et al. [2018] stating that 'volatility is rough' because

In this thesis we also introduce a third roughness estimator, the sequential scale estimator $\widehat{\mathscr{R}}_n^s$ first introduced by Han and Schied [2023]. This estimator esti-

mates the roughness of a path from discrete observations of integrated variance or realized variance and is developed with the purpose of minimizing the possible distortion caused by estimation errors. We find that by modifying the estimator into the absolute sequential scale estimator $|\widehat{\mathscr{R}}_n^s|$ we do obtain more accurate estimates from realized data compared to our other two roughness estimators. For our two stochastic diffusive models in section 4.1 and 4.2, $|\widehat{\mathscr{R}}_n^s|$ performs very well when using realized variance as input, and it accurately estimates the true roughness of the underlying model $H = \frac{1}{2}$. Thus, in these two examples $|\widehat{\mathscr{R}}_n^s|$ completely remedies the apparent rough behaviour of realized volatility. However, for our models driven by a fractional Ornstein-Uhlenbeck model in section 4.3 and 4.4, the absolute sequential scale estimator does not perform as well as before. Here we find that $|\widehat{\mathscr{R}}_n^s|$ tends to always estimate the roughness of realized variance near 0.5 when the underlying model is actually smooth (i.e. $H > \frac{1}{2}$). When the underlying model is rough (i.e. $H < \frac{1}{2}$) $|\widehat{\mathscr{R}}_n^s|$ tends to overestimate the true roughness such that it in all cases estimates the path to be nearer to diffusive behaviour (i.e. $H = \frac{1}{2}$) than the true model actually is.
When we instead of realized variance use integrated variance computed directly from instantaneous volatility $\sigma_t$ as input, the sequential scale estimator performs very well, and does in all cases estimate the true roughness of the model accurately. Thus, $|\widehat{\mathscr{R}}_n^s|$ is also vulnerable to estimation errors where estimation error in this case means the difference between realized variance and integrated variance.

Comparing our three roughness estimators we find that they all perform very well in our examples when based on instantaneous volatility. $\widehat{H}_{L,K}$ and $|\widehat{\mathscr{R}}_n^s|$ work in a model-free setting and are therefore very flexible and applicable to many different models. Estimators like $\widehat{H}_R$ only works well if the class of models is well-specified. However, $\widehat{H}_R$ seems to converge faster, and it requires less data input for the estimate to be accurate.
For realized volatility/variance $|\widehat{\mathscr{R}}_n^s|$ does in some cases perform much better than the other two estimators, but it does not estimate the roughness of the underlying model accurately in all cases. Furthermore, $|\widehat{\mathscr{R}}_n^s|$ has much stronger requirements to the input data, and it needs observations at very specific time points. That makes the estimator less applicable to real world high-frequency data where the discrete grid of observation times might not be a uniform partition sequence.

For future investigation it could be relevant to investigate how the absolute sequential scale estimator $|\widehat{\mathscr{R}}_n^s|$ could be further improved. The estimation error for this estimator is as shown very small, and if the estimator could fully handle this estimation error it has the potential to perform reliable roughness estimates from realized data. Another thing that could be further investigated is the estimation error itself. If it turns out that the estimation error is insignificant when using a certain approach to calculate it or a certain set of models, it would shed light on when to expect reliable roughness estimates. Both of these things could be a helping tool in determining whether volatility is rough or not.

# 6 Appendix

## 6.1 Simulation of fractional Brownian motion

Throughout this thesis we will be simulating from the fractional Brownian motion by using a spectral method which can be used for stationary processes. The idea is to analyse the stochastic process in the spectral domain rather than the time domain. The spectral density is computed as follows for frequencies $-\pi \leq \lambda \leq \pi$:

$$f(\lambda) := \sum_{j=-\infty}^{\infty} \gamma(j) \exp(ij\lambda) \tag{22}$$

where $\gamma(\cdot)$ represent the autocovariance function. It can be shown that the spectral density of fractional Gaussian noise is given by

$$f(\lambda) = 2\sin(\pi H)\Gamma(2H+1)(1-\cos\lambda)[|\lambda|^{-2H-1} + B(\lambda, H)] \tag{23}$$

where $\Gamma(\cdot)$ denotes the Gamma function and

$$B(\lambda, H) := \sum_{j=1}^{\infty} \left((2\pi j + \lambda)^{-2H-1} + (2\pi j - \lambda)^{-2H-1}\right) \tag{24}$$

for $-\pi \leq \lambda \leq \pi$. The infinite sum makes direct numerical evaluation almost impossible. However, a useful approximation of the sum is made by Paxson [1997]. They show that by using

$$\tilde{B}_3(\lambda, H) := \sum_{j=1}^{3} \left(\left(a_j^+\right)^{-2H-1} + \left(a_j^-\right)^{-2H-1}\right) + \frac{\left(a_3^+\right)^{-2H} + \left(a_3^-\right)^{-2H} + \left(a_4^+\right)^{-2H} + \left(a_4^-\right)^{-2H}}{8H\pi}$$

where $a_j^{\pm} = 2\pi j \pm \lambda$, $f(\lambda)$ is approximated quite well.

Now, consider a stationary Gaussian discrete-time process $X = \{X_n : n = 0, ..., N-1\}$ where $N$ is the required sample size. The spectral theorem states that it can be represented in terms of the spectral density as

$$X_n \stackrel{d}{=} \int_0^{\pi} \sqrt{\frac{f(\lambda)}{\pi}} \cos(n\lambda) dB_1(\lambda) - \int_0^{\pi} \sqrt{\frac{f(\lambda)}{\pi}} \sin(n\lambda) dB_2(\lambda) \tag{25}$$

where $B_1$ and $B_2$ are two mutually independent Brownian motions Dieker and Mandjes [2003]. We wish to approximate (8). The integrand is replaced by a simpler function. Fix some integer $l$ and set $t_k = \pi k/l$ for $k = 0, ..., l$. Now, define a simple function $\xi_n^{(l)}$ on $[0, \pi]$ for $0 \leq n \leq N-1$ by

$$\xi_n^{(\ell)}(\lambda) = \sqrt{\frac{f(t_1)}{\pi}} \cos(nt_1) \mathbf{1}_{\{0\}}(\lambda) + \sum_{k=0}^{l-1} \sqrt{\frac{f(t_{k+1})}{\pi}} \cos(nt_{k+1}) \mathbf{1}_{(t_k, t_{k+1}]}(\lambda). \tag{26}$$

The first integral in (8) can be approximated by $\int_0^\pi \xi_n^{(\ell)}(\lambda)dB_1(\lambda)$. Since $\xi_n^{(\ell)}$ is a simple function the stochastic integral can be computed as

$$\int_0^\pi \xi_n^{(l)}(\lambda)dB_1(\lambda) = \sum_{j=0}^{\ell-1} \xi_n^{(l)}(B(t_{j+1}) - B(t_j)). \tag{27}$$

Thus, we obtain

$$\int_0^\pi \xi_n^{(l)}(\lambda)dB_1(\lambda) = \sum_{j=0}^{\ell-1}\sum_{k=0}^{\ell-1} \sqrt{\frac{f(t_{k+1})}{\pi}} \cos(nt_{k+1})\mathbf{1}_{(t_k,t_{k+1}]}(B_1(t_{j+1}) - B_1(t_j))$$
$$= \sum_{k=0}^{l-1} \sqrt{\frac{f(t_{k+1})}{\pi}} \cos(nt_{k+1})(B_1(t_{k+1}) - B_1(t_k))$$
$$= \sum_{k=0}^{\ell-1} \sqrt{\frac{f(t_{k+1})}{\pi}} \cos(nt_{k+1})U_k^{(0)}\sqrt{\frac{\pi}{l}} = \sum_{k=0}^{\ell-1} \sqrt{\frac{f(t_{k+1})}{\ell}} \cos(nt_{k+1})U_k^{(0)}$$

where $U_k^{(0)}$ is an i.i.d. standard normal random variable for $k = 0, ..., \ell-1$. The $U_k^{(0)}\sqrt{\pi/\ell}$ represent the Brownian motion increments which per definition are normally distributed with mean 0 and variance $t_{k+1} - t_k$.

The second integral in (8) can be approximated in a similar way by replacing the cosine terms with sine terms. Thus, we obtain the following approximation of $X_n$:

$$\hat{X}_n^{(\ell)} := \sum_{k=0}^{\ell-1} \sqrt{\frac{f(t_{k+1})}{\ell}} \left(\cos(nt_{k+1})U_k^{(0)} - \sin(nt_{k+1})U_k^{(1)}\right). \tag{28}$$

The two vectors $U^{(0)}$ and $U^{(1)}$ are mutually independent since $B_1$ and $B_2$ are independent as well. In order to calculate $\hat{X}_n^{(\ell)}$ efficiently we will be using the fast Fourier transform (FFT). To this end, we define the sequence $(a_k)_{k=0,\ldots,2\ell-1}$ by

$$a_k := \begin{cases} 0 & k = 0; \\ \frac{1}{2}\left(U_{k-1}^{(0)} + iU_{k-1}^{(1)}\right)\sqrt{\frac{f(t_k)}{\ell}} & k = 1, \ldots, \ell-1; \\ U_{k-1}^{(0)}\sqrt{\frac{f(t_k)}{\ell}} & k = \ell; \\ \frac{1}{2}\left(U_{2\ell-k-1}^{(0)} - iU_{2\ell-k-1}^{(1)}\right)\sqrt{\frac{f(t_{2\ell-k})}{\ell}} & k = \ell+1, \ldots, 2\ell-1. \end{cases}$$

It is shown in Appendix 6.1.1 that the Fourier transform of $a_k$ is indeed real and equals $\hat{X}_n^{(\ell)}$. From this approximated fractional Gaussian noise we can generate the fBm.

Dieker and Mandjes [2003] shows that the finite-dimensional distributions of $\hat{X}^{(\ell)}$ converge in probability to the corresponding finite-dimensional distributions of $X$ as $\ell \to \infty$. The rate of convergence is, however, quite slow. Therefore, we will be using a $\ell \geq 30000$ when simulating from the fBm by the spectral method in this thesis in order to make sure that our simulations are reliable. Figure 27 shows three simulations of fractional Brownian motions with different Hurst parameters generated by the spectral method.

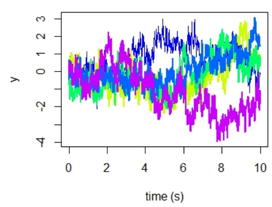


(a) H=0.2

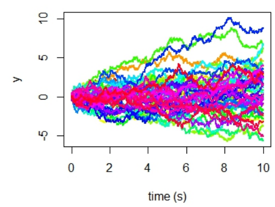


(b) H=0.5

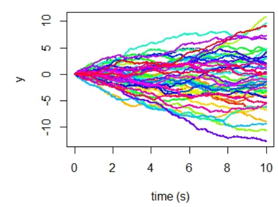


(c) H=0.8

Figure 27: Fractional Brownian motions generated by the spectral method.

### 6.1.1 Proof of Fourier transform in spectral method

Consider

$$a_k := \begin{cases} 0 & k = 0; \\ \frac{1}{2}\left(U_{k-1}^{(0)} + iU_{k-1}^{(1)}\right)\sqrt{\frac{f(t_k)}{\ell}} & k = 1, \dots, \ell - 1; \\ U_{k-1}^{(0)}\sqrt{\frac{f(t_k)}{\ell}} & k = \ell; \\ \frac{1}{2}\left(U_{2\ell-k-1}^{(0)} - iU_{2\ell-k-1}^{(1)}\right)\sqrt{\frac{f(t_{2\ell-k})}{\ell}} & k = \ell + 1, \dots, 2\ell - 1. \end{cases}$$

We want to take the Fourier transform of this sequence. The Fourier transform of $(a_k)_{k=0}^{2\ell-1}$ is $\lambda_n = \sum_{k=0}^{2\ell-1} a_k \exp(2\pi i \frac{nk}{2\ell})$. By Euler's formula we obtain

$$\lambda_n = \sum_{k=0}^{2\ell-1} a_k \left(\cos\left(\pi\frac{nk}{\ell}\right) + i \sin\left(\pi\frac{nk}{\ell}\right)\right).$$

We will now insert $a_k$ and split the sum into the four different cases of $a_k$. Hence, we obtain

$$\lambda_n = 0 + \sum_{k=1}^{l-1} \frac{1}{2} \left( U_{k-1}^{(0)} + iU_{k-1}^{(1)} \right) \sqrt{\frac{f(t_k)}{\ell}} \left( \cos\left(\pi \frac{nk}{\ell}\right) + i \sin\left(\pi \frac{nk}{\ell}\right) \right)$$
$$+ U_{\ell-1}^{(0)} \sqrt{\frac{f(t_\ell)}{\ell}} \left( \cos\left(\pi \frac{n\ell}{\ell}\right) + i \sin\left(\pi \frac{n\ell}{\ell}\right) \right)$$
$$+ \sum_{k=l+1}^{2l-1} \frac{1}{2} \left( U_{2\ell-k-1}^{(0)} - iU_{2\ell-k-1}^{(1)} \right) \sqrt{\frac{f(t_{2\ell-k})}{\ell}} \left( \cos\left(\pi \frac{nk}{\ell}\right) + i \sin\left(\pi \frac{nk}{\ell}\right) \right).$$

By definition $t_k = \frac{\pi k}{\ell}$. Thus, what is inside the cosine and sine functions is simply $nt_k$. Note that for $k = \ell$ we have $t_k = \pi$. Thus, $\sin(nt_\ell) = 0$ since $n$ is an integer. By inserting this and changing the indexes of the two sums, we obtain

$$\lambda_n = U_{\ell-1}^{(0)} \sqrt{\frac{f(t_\ell)}{\ell}} \cos(nt_\ell)$$
$$+ \sum_{k=0}^{l-2} \frac{1}{2} \left( U_k^{(0)} + iU_k^{(1)} \right) \sqrt{\frac{f(t_{k+1})}{\ell}} \left( \cos(nt_{k+1}) + i \sin(nt_{k+1}) \right)$$
$$+ \sum_{k=0}^{l-2} \frac{1}{2} \left( U_{\ell-k-2}^{(0)} - iU_{\ell-k-2}^{(1)} \right) \sqrt{\frac{f(t_{\ell-k-1})}{\ell}} \left( \cos(nt_{\ell+k+1}) + i \sin(nt_{\ell+k+1}) \right).$$

Now note that $\sin(nt_{\ell+k+1}) = -\sin(nt_{\ell-(k+1)})$ since $t_\ell = \pi$. Similarly, $\cos(nt_{\ell+k+1}) = \cos(nt_{\ell-(k+1)})$. By inserting that in the last sum in the above expression, the sum becomes

$$\sum_{k=0}^{l-2} \frac{1}{2} \left( U_{\ell-k-2}^{(0)} - iU_{\ell-k-2}^{(1)} \right) \sqrt{\frac{f(t_{\ell-k-1})}{\ell}} \left( \cos(nt_{\ell-k-1}) - i \sin(nt_{\ell-k-1}) \right)$$
$$= \sum_{k=0}^{l-2} \frac{1}{2} \left( U_k^{(0)} - iU_k^{(1)} \right) \sqrt{\frac{f(t_{k+1})}{\ell}} \left( \cos(nt_{k+1}) - i \sin(nt_{k+1}) \right)$$

where we have reversed the sum order. Now we can combine the two sums into one. Several terms cancel out such that we obtain

$$\lambda_n = U_{\ell-1}^{(0)} \sqrt{\frac{f(t_\ell)}{\ell}} \cos(nt_\ell) + \sqrt{\frac{f(t_{k+1})}{\ell}} \sum_{k=0}^{l-2} \left( U_k^{(0)} \cos(nt_{k+1}) - U_k^{(1)} \sin(nt_{k+1}) \right)$$
$$= \sum_{k=0}^{l-1} \sqrt{\frac{f(t_{k+1})}{\ell}} \left( U_k^{(0)} \cos(nt_{k+1}) - U_k^{(1)} \sin(nt_{k+1}) \right)$$

which equals the definition of $\hat{X}_n^{(\ell)}$ from (28) as desired.

## References


Christian Bayer, Peter Friz, and Jim Gatheral. Pricing under rough volatility. *Quantitative Finance*, 16(6):887–904, 2016.

F Biagini. Stochastic calculus for fractional brow-nian motion and applications. *Probability and its Applications (New York)/SpringerVerlag London, Ltd*, 2008.

Anine E Bolko, Kim Christensen, Mikko S Pakkanen, and Bezirgen Veliyev. A gmm approach to estimate the roughness of stochastic volatility. *Journal of Econometrics*, 235(2):745–778, 2023.

Tim Bollerslev and Hans Ole Mikkelsen. Modeling and pricing long memory in stock market volatility. *Journal of econometrics*, 73(1):151–184, 1996.

Fabienne Comte and Eric Renault. Long memory in continuous-time stochastic volatility models. *Mathematical finance*, 8(4):291–323, 1998.

Rama Cont and Purba Das. Rough volatility: fact or artefact? *Sankhya B*, 86 (1):191–223, 2024.

Antonius Bernardus Dieker and Michael Mandjes. On spectral simulation of fractional brownian motion. *Probability in the Engineering and Informational Sciences*, 17(3):417–434, 2003.

Omar El Euch, Jim Gatheral, and Mathieu Rosenbaum. Roughening heston. *Risk*, pages 84–89, 2019.

Masaaki Fukasawa, Tetsuya Takabatake, and Rebecca Westphal. Consistent estimation for fractional stochastic volatility model under high-frequency asymptotics. *Mathematical Finance*, 32(4):1086–1132, 2022.

Jim Gatheral, Thibault Jaisson, and Mathieu Rosenbaum. Volatility is rough. *Quantitative finance*, 18(6):933–949, 2018.

Xiyue Han and Alexander Schied. The hurst roughness exponent and its model-free estimation, 2022a.

Xiyue Han and Alexander Schied. Robust faber–schauder approximation based on discrete observations of an antiderivative. *arXiv preprint arXiv:2211.11907*, 2022b.

Xiyue Han and Alexander Schied. Estimating the roughness exponent of stochastic volatility from discrete observations of the realized variance. *arXiv preprint arXiv:2307.02582*, 2023.

Jean Jacod. *Discretization of processes*. Springer, 2012.

Vern Paxson. Fast, approximate synthesis of fractional gaussian noise for generating self-similar network traffic. *ACM SIGCOMM Computer Communication Review*, 27(5):5–18, 1997.